HHS Public Access

Author manuscript

Cell. Author manuscript; available in PMC 2022 November 11.

Published in final edited form as:

Cell. 2021 November 11; 184(23): 5715–5727.e12. doi:10.1016/j.cell.2021.10.004.

Enteric pathogens induce tissue tolerance and prevent neuronal loss from subsequent infections

Tomasz Ahrends[1], **Begüm Aydin**[1], **Fanny Matheis**[1], **Cajsa H. Classon**[1,2], **François Marchildon**[3], **Gláucia C. Furtado**[4], **Sérgio A. Lira**[4], **Daniel Mucida**[1,5]

[1]Laboratory of Mucosal Immunology, The Rockefeller University, New York, NY, USA.

[2]Present address: Laboratory of Development and Homeostasis of the Nervous System, The Francis Crick Institute, London, UK.

[3]Laboratory of Molecular Metabolism, The Rockefeller University, New York, NY, USA.

[4]Precision Immunology Institute, Icahn School of Medicine at Mount Sinai, New York, NY, USA.

[5]Howard Hughes Medical Institute, The Rockefeller University, New York, NY, USA

Summary

The enteric nervous system (ENS) controls several intestinal functions including motility and nutrient handling, which can be disrupted by infection-induced neuropathies or neuronal cell death. We investigated possible tolerance mechanisms preventing neuronal loss and disruption in gut motility after pathogen exposure. We found that following enteric infections, muscularis macrophages (MMs) acquire a tissue-protective phenotype that prevents neuronal loss, dysmotility and maintain energy balance during subsequent challenge with unrelated pathogens. Bacteria-induced neuroprotection relied on activation of gut-projecting sympathetic neurons and signaling via β_2-adrenergic receptors (β2AR) on MMs. In contrast, helminth-mediated neuroprotection was dependent on T cells and systemic production of interleukin (IL)-4 and -13 by eosinophils, which induced arginase-expressing MMs that prevented neuronal loss from an unrelated infection located in a different intestinal region. Collectively, these data suggest that distinct enteric pathogens trigger a state of disease- or tissue tolerance that preserves ENS number and functionality.

Correspondence should be addressed to T.A. (tahrends@rockefeller.edu) or to D.M. (mucida@rockefeller.edu).
Lead contact: D.M.

Author Contributions

T.A. initiated, designed, performed the research and wrote the manuscript. B. A., F.M. (CLAMS cages) and C.C. designed and performed experiments. G.F., S.L. generated the cpa3$^{DTR\text{-}tdTomato}$ mice. D.M. conceived, initiated, designed, supervised the research, and wrote the manuscript. All authors revised and edited the manuscript and figures.

Declaration of interests

The authors declare no competing interests.

Inclusion and diversity statement

We worked to ensure sex balance in the selection of non-human subjects. One or more of the authors of this paper self-identifies as an underrepresented ethnic minority in science. One or more of the authors of this paper self-identifies as a member of the LGBTQ+ community. While citing references scientifically relevant for this work, we also actively worked to promote gender balance in our reference list.

Graphical Abstract

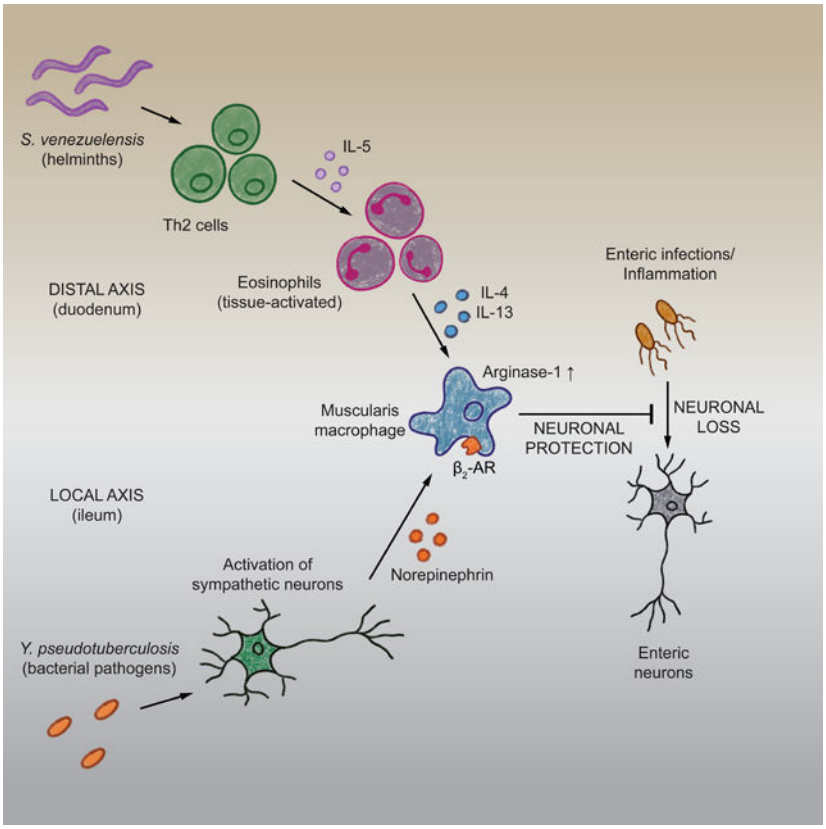

eTOC Blurb:

Bacterial and helminth pathogens in the intestine induce distinct pathways converging on tissue macrophages that mediate enteric neuronal protection, aiding host fitness via intestinal motility and energy balance during subsequent infections.

Introduction

The gastrointestinal (GI) tract needs to simultaneously generate tolerance to harmless or beneficial dietary and microbial antigens and resistance to pathogen invasion. Additionally, disease tolerance to pathogen- and inflammation-induced tissue damage must operate in the intestine to maintain homeostasis (Medzhitov et al., 2012; Soares et al., 2014). This is particularly relevant for cells with reduced proliferative or regenerative capacity, such as enteric neurons, which are abundantly present in the gut and serve to modulate intestinal motility and secretory function (Balemans et al., 2017; Furness et al., 2013; O'Leary et al., 2019).

Previous studies in mice and rats, supported by clinical observations, indicate enteric infections can lead to neuronal loss, long-term dysmotility and neuropathies (Holschneider et al., 2011; Matheis et al., 2020; Ohman and Simren, 2010; White et al., 2018). Yet,

whether a state of tolerance can be induced after exposure to pathogens, preventing cumulative neuronal loss and functional changes, is still not known.

We investigated possible tolerance mechanisms preventing neuronal loss and disruption in gut motility after pathogen exposure. We found that following helminth or bacterial infection and via distinct pathways MMs acquire tissue-protective qualities and prevent neuronal loss during subsequent challenge with an unrelated pathogen. Collectively, our data suggest that distinct enteric pathogens trigger a state of tolerance aimed to preserve the numbers and functionality of the ENS.

Results

Y. pseudotuberculosis infection induces enteric neuron protection during subsequent infection.

To test whether primary infection can prevent neuronal loss after secondary challenge with an unrelated pathogen, we used an attenuated strain of *Salmonella* Typhimurium, *spiB*, which harbors a mutation in the type-III secretion system, impacting its intracellular replication (Tsolis et al., 1999). In contrast to wild-type *Salmonella*, *spiB* is not lethal and is cleared from wild-type C57BL/6 mice in 7–10 days, inducing a less severe form of Salmonellosis; nevertheless, *spiB* infection is sufficient to induce rapid neuronal loss and long-term dysmotility (Matheis *et al.*, 2020). We thus first asked whether primary infection with an unrelated bacterium influences the tissue's response to a subsequent exposure to *spiB*. We used *Yersinia pseudotuberculosis* (*Yp*), which like *Salmonella*, is a foodborne Gram-negative bacterium that primarily localizes to the ileum (Fonseca et al., 2015), causing a transient infection undetectable in the feces by 21 days post-infection (dpi) (Figure 1A). Primary infection with *Yp* led to significant neuronal loss, however not as pronounced as after primary *spiB* infection. Additionally, as suggested by our recent studies (Matheis *et al.*, 2020), *spiB* exposure following an earlier *Yp* infection did not result in further neuronal loss (Figure 1B). This was not a result of an improved resistance to *spiB* as mice previously infected with *Yp* displayed similar pathogen load and clearance pattern to naïve mice (Figure 1C).

Disease tolerance strategies alleviate the fitness costs by promoting resilience in the presence of an insult (Ayres, 2020). Because one of the main roles of the ENS regarding fitness cost is the control of intestinal motility, we measured GI transit time as a functional readout for neuronal loss. Decreased enteric neuron numbers generally correlated with increased GI transit time; while *spiB* infection led to increased GI transit time, previous *Yp* infection preserved gut motility after subsequent *spiB* challenge (Figure 1D). These results point to development of tissue-, or disease tolerance (Ayres, 2020; Martins et al., 2019) post-bacterial infection, which prevented neuronal loss to subsequent infection with a different pathogen.

We have previously shown that MMs quickly acquire a tissue-protective phenotype and limit enteric neuron loss during primary *spiB* infection via β_2 adrenergic receptor (β_2-AR) signaling and Arginase 1-dependent polyamine production by MMs (Gabanyi et al., 2016; Matheis *et al.*, 2020). To test whether *Yp*-induced tolerance relied on MMs, we used

anti-CSF1R antibody, which selectively depletes MMs while preserving lamina propria macrophages (LpM) when administered at 50 mg/kg, and does not affect neuronal numbers (Matheis *et al.*, 2020; Muller et al., 2014), as opposed to long-term steady-state macrophage depletion (De Schepper et al., 2018). Administration of anti-CSF1R antibody to mice post *Yp* clearance led to a pronounced neuronal loss following challenge with *spiB*, suggesting the requirement for MMs to maintain *Yp*-induced neuronal protection (Figure 1E). Flow cytometric analysis of the ileum from mice after primary infection revealed that *Yp* infection leads to the upregulation of Arg1 by MMs beyond a basal level (Figures 1F and 1G). To examine whether heightened Arg1 expression by MMs is required for *Yp*-induced neuroprotection, we used LysM$^{\Delta Arg1}$ mice, in which *Arg1* is conditionally deleted in myeloid cells. *Yp*-mediated neuroprotection was abolished in LysM$^{\Delta Arg1}$ following challenge with *spiB* infection (Figure 1H). Moreover, this neuroprotective mechanism also required β_2-AR expression by MMs, as LysM$^{\Delta Adrb2}$ mice previously infected with *Yp* showed significant neuronal loss compared to wild-type littermate control mice upon *spiB* infection (Figure 1I). This effect correlated with decreased Arg1 expression by MMs and increased GI transit-time (Figure 1J and 1K). Consistently, while disease tolerance was impaired by both Arg1 and β_2-AR targeting on MMs, *spiB* load was not affected by these strategies (Figures S1A and S1B). These results indicate that primary bacterial infection results in a state of disease tolerance that mediates neuroprotection to subsequent infections, preserving intestinal motility.

Helminth infections induce long-term neuronal protection during subsequent infection.

Next, we asked whether infection-induced neuroprotection could be induced by other pathogens. We aimed to determine whether helminths, which co-evolved with mammals and typically induce a very distinct immune response to bacterial pathogens, could prevent neuronal loss. We chose to infect mice with *Strongyloides venezulenesis* (*Sv*), a parasitic nematode that causes an acute infection and primarily localizes to the duodenum (Esterhazy et al., 2019; Silveira et al., 2002). Initial *Sv* infection was cleared by 12 dpi and, contrary to the bacterial pathogens we tested, it did not lead to neuronal loss in the ileum or duodenum (Figures 2A, 2B, S2A, and (Matheis *et al.*, 2020)). However, primary *Sv* duodenum infection completely prevented neuronal loss in the ileum and colon following subsequent *spiB* challenge (Figures 2B and S2B). This distal protection by previous, proximal *Sv* infection was not associated with changes in *spiB* load and resulted in the maintenance of normal gut motility (Figures 2C and 2D).

We addressed whether enteric neuronal loss-associated dysmotility also affected feeding behavior and activity of mice. Using CLAMS or metabolic cages, we found that *spiB* challenge resulted in higher food intake in *spiB*-infected mice that had not been previously infected with *Sv*; changes that did not translate into higher weight (Figures S2C and S2D). Moreover, *spiB* infection led to higher ambulatory activity and increased energy balance, all of which were prevented by initial *Sv* infection (Figures S2E and S2F). These observations point to a deficient nutrient absorption in *spiB*-infected mice, possibly associated with the loss of enteric neurons and prevented by previous helminth infection. While the proximal intestine-helminth *Heligmosomoides polygyrus* (*Hp*) was recently shown to impair anti-neurotropic virus immunity (Desai et al., 2021), we observed distal protection from neuronal

loss in the ileum in *Hp*-infected and ivermectin-treated mice subsequently infected with *spiB* (Figure S2G). Moreover, initial *Sv* infection also led to neuroprotection after subsequent *Yp* challenge (Figure S2H). Consistent with a disease tolerance phenotype, primary *Sv* or *Hp* infection did not affect subsequent clearance of *spiB* or *Yp*, respectively (Figures S2I and S2J).

Sv-induced tolerance depended on MMs, as evidenced by anti-CSF1R antibody-mediated depletion of MMs post *Sv* clearance, which abolished the neuroprotection upon *spiB* infection (Figure 2E). Following *Sv* challenge ~80% of MMs expressed Arg1, compared to ~60% observed after *spiB* infection (Figure 2F and S2F). MMs in the duodenum expressed heightened Arg1 already at steady state compared to the ileum, and this was not further increased following *spiB* or *Sv* infection (Figure S2K). *Sv* infection also influenced mucosal macrophages beyond the site of infection, evidenced by increased frequencies of Arg1+ MMs in colon and lung, but did not change arginase-1 expression by spleen macrophages (Figures S2L–S2N). In contrast to wild-type mice, LysM$^{\Delta Arg1}$ mice infected with *Sv* displayed neuronal loss, which was nevertheless maintained upon subsequent *spiB* infection (Figure 2G). In opposition to *Yp*, *Sv* infection did not result in activation of gut-projecting sympathetic neurons (Figure 2H). In contrast to the phenotype observed post *Yp*, *Sv*-mediated neuronal protection to subsequent *spiB* infection was maintained in LysM$^{\Delta Adrb2}$ mice. Mice lacking β_2-AR signaling in myeloid cells previously infected with *Sv* also sustained similar neuronal numbers, Arg1 expression by MMs, and GI transit time upon *spiB* infection as wild-type littermate controls (Figures 2I–2K). Moreover, initial infection with *Sv* did not affect *spiB* load and clearance in either LysM$^{\Delta Adrb2}$ and LysM$^{\Delta Arg1}$ mice (Figures S2O and S2P). These results indicate that while converging on neuroprotective MMs, *Yp*- and *Sv*-induced disease tolerance mechanisms are distinct.

We also examined how long *Sv*-mediated neuroprotection is maintained after the initial infection is cleared. Subsequent *spiB* challenge up to 12 weeks after primary *Sv* infection did not result in any neuronal loss. Challenge at 24 weeks post-infection did result in significant neuronal loss, however the enteric neuron numbers were still higher when compared to controls infected with *spiB* only. (Figure 2L). Long-term enteric neuron protection correlated with sustained high expression of Arg1 in MMs observed up to 12 weeks post-infection (Figure 2M). These results reveal a long-term neuroprotection in the ileum induced by a single duodenal helminth infection.

Finally, we performed transcriptomic analysis of ileum MMs isolated from non-infected mice or from mice infected with *spiB*, *Yp* or *Sv*. Comparison between different infections resulted in a low number differentially regulated genes, indicating a significant overlap in MM phenotype induced by different types of enteric infection (Figures 3A–3C). Comparison of gene expression profiles between MMs isolated from all infected versus non-infected mice revealed a broad tissue-protective signature which include wound healing genes, characteristic of alternatively-activated macrophages (Figure 3D and Table S1), confirming and extending our previous observations (Gabanyi *et al.*, 2016). This gene signature was highly enriched in previously published transcriptomic data from human “alternatively-activated” (Pello et al., 2012) and “tolerogenic macrophages” (Mages et al., 2007) (Figures 3E and 3F). These data indicate that regardless of the type of infection, proximal versus

distal upstream stimuli, MMs acquire a default tissue-protective gene signature, resembling murine and human ‘M2-like’ phenotype.

Immune response to *S. venezuelensis* is associated with neuronal protection during subsequent infection.

To identify a mechanism responsible for the long-term helminth–driven disease tolerance, we further characterized the immune response to *Sv*. Helminths are known to drive a robust type-2 immunity, with accumulation of innate immune cells, including tuft cells, eosinophils and group 2 innate lymphoid cells (ILC2), and later $CD4^+$ T helper 2 (T_h2) cells (Maizels, 2020; O’Leary *et al.*, 2019; Vivier et al., 2018). Coinfections with helminths may result in deviation of appropriate immune responses resulting in breakdown of barrier and increased susceptibility to unrelated pathogens (Desai *et al.*, 2021; Marple et al., 2017). We observed an accumulation of $Gata3^+$ $CD4^+$ “T_h2” cells in the duodenum, but not in the ileum LP following *Sv* infection, which was further increased when mice underwent subsequent *spiB* infection (Figures 4A and S3A). Additionally, we found a significant increase in the frequencies of mucosal mast cells and eosinophils in the LP and intraepithelial (IE) compartments of the ileum and duodenum of *Sv*-infected mice (Figures 4B, 4C, S3B, and S3C). At steady-state, however, the duodenum harbored higher numbers of eosinophils than the ileum, the former reaching almost 80% of total $CD45^+$ cells found in the LP post *Sv*-infection (Figures 4B and 4C). Of note, duodenal eosinophilia was maintained for up to 12 weeks post-infection and diminished at week 24 (Figure 4D), reflecting changes observed in MMs, GI transit time and neuroprotection post-*Sv* infection described above. Consistent with an overall heightened type-2 immunity, serum of *Sv*-infected mice showed prolonged increase in interleukin (IL)-4 and IL-13 levels (Figures 4E and 4F) that were not affected by subsequent *spiB* infection (Figure S3D).

We next examined whether $CD4^+$ T cells were required for *Sv*-induced neuroprotection using a depleting anti-CD4 antibody following primary infection (Figure 4G). Depletion of CD4-expressing cells hindered type-2 immunity and the capacity to clear *Sv* infection. Therefore, we treated mice with the anti-helminthic drug, ivermectin, before infecting them with *spiB*, which on its own did not lead to neuronal loss (Figure 4H and S3E). Mice treated with anti-CD4 antibody showed significant neuronal loss, which correlated with reduced eosinophilia and Arg1 expression by MMs (Figures 4I–4K). Tissue-resident memory T (T_{RM}) cells mediate important *in situ* resistance functions and were also shown to provide cross-protection against different pathogens (Ariotti et al., 2014). We examined their role in *Sv*-induced neuroprotection by using mice with selective deficiency in the transcription factors Hobit and Blimp-1 (DKO mice), which were shown to be unable to generate T_{RM} cells (Mackay et al., 2016). Compared to wild-type controls, DKO mice displayed no differences in neuron numbers, frequencies of eosinophils and Arg1-expressing MMs after successive exposure to *Sv* and *spiB*, suggesting that T_{RM} cells do not play a significant role in this process (Figures S3F–S3H). These results indicate that $CD4^+$ T cells are required for *Sv*-induced neuroprotection and point to their “accessory” or “helper” role in this process.

We then assessed whether the two main innate immune cell types that accumulate during helminth infections, mast cells and eosinophils, play a role in *Sv*-induced neuroprotection.

Mast cell accumulation after *Sv* infection was predominantly observed in the duodenum epithelial compartment (Figure S3B). To target mast cells, we generated a novel CRISPR-based *knock-in* strain in which human diphtheria toxin receptor (hDTR) and the td tomato fluorescent protein are expressed under a promoter preferentially active in mast cells and in a subset of basophils (Lilla et al., 2011), carboxypeptidase A3 (*cpa3*). Administration of diphtheria toxin (DT) after initial *Sv* infection led to a significant reduction in mast cell numbers (Figure S3I). Consistent with a role for mast cells in resistance to helminths, DT-treated mice showed a significant delay in Sv clearance (Figure S3J). Nevertheless, *Sv*-infected DT-treated *cpa3*$^{\text{DTR-tdTomato}}$ and control mice showed similar enteric neuron numbers upon subsequent *spiB* challenge, suggesting that mast cells are dispensable for neuroprotection (Figure S3K).

To address a possible role for eosinophils in this process, we first treated *Sv*-infected mice with neutralizing anti-IL-5 antibody followed by *spiB* infection. ILC2- and Th2-derived IL-5 drives eosinophil activation and accumulation (Maizels, 2020; O'Leary *et al.*, 2019; Vivier *et al.*, 2018); consistently, following *Sv* infection the frequencies of ILC2s and IL-5-producing CD4^{+} T cells in duodenum LP were elevated and IL-5 blockade resulted in impaired eosinophilia (Figures 3L and S3L–S3N). Additionally, *Sv*-infected mice treated with anti-IL-5 displayed a significant neuronal loss and reduced Arg1 expression by MMs upon subsequent *spiB* exposure (Figures S3O and S3P). This data points to an important role for eosinophils in neuroprotection and disease tolerance post helminth infection.

Pet store mice are resistant to neuronal loss upon *spiB* infection.

We next turned to potential implications of infection-induced neuroprotection in free-living or non-laboratory organisms, which are exposed to more pathogens and sustain a higher immune activation than laboratory animals (Abolins et al., 2017). We asked whether increased exposure to pathogens in mice maintained in a pet store resulted in altered enteric neuron numbers at steady state and loss upon bacterial infection. At steady state, pet store mice displayed lower neuronal numbers per mm^2 when compared to naïve specific-pathogen-free (SPF) C57BL/6 mice (Figure 5A), resembling what we observed in SPF mice previously infected with *Yp*. However, we observed that pet store mice had significantly longer small intestines (Figure 5B). To account for these morphological differences, we analyzed the numbers of neurons found in each ganglion. Pet store mice had similar numbers of neurons per ganglion when compared to non-infected SPF controls (Figure 5C). Nevertheless, infection with *spiB* resulted in a decrease of both total number and neurons per ganglia in SPF, but not in pet store mice, although the latter also cleared *spiB* two days earlier than average SPF mice (Figures 5A, 5C and 5D). We noted a wide range in the frequency of eosinophils in the LP of pet store mice, probably reflecting their varied infection history (Figure 5E). Additionally, pet store mice showed overall elevated levels of serum IL-4 and IL-13, and Arg1 expression by MMs (Figures 5F and 5G). Finally, consistently with the increased frequency of eosinophils in the tissue, analysis of bone marrow of pet store mice revealed that both hematopoietic progenitors (Lineage^{-}Sca1^{+}c-Kit^{+}, LSK) cells and eosinophil progenitor (EoP) cells were enriched when compared to SPF controls (Figures 5H–5J). The mixed genetic background of pet store mice might contribute to the spread observed in this group. To independently address whether a

skewed type-2 immune response prior to infection influence neuronal loss upon enteric infections, we analyzed syngeneic SPF BALB/c mice, known to exhibit “Th2-dominant immune responses” (Iniesta et al., 2002). Indeed, BALB/c mice displayed higher frequency of Arg1+ MMs in the ileum than C57BL/6 counterparts and no significant neuronal loss upon *spiB* infection, indicating that genetic makeup comprises an essential component in neuro-immune responses to infection (Figures 5K and 5L). Overall, the above data suggest that both infection history and genetic makeup contribute to long-term protective mechanisms that regulate or prevent neuronal loss during enteric infections occurring in life.

IL-4– and IL-13–producing eosinophils mediate *Sv*-induced neuronal protection.

To directly investigate the contribution of eosinophils to this process, we utilized a genetic mouse model in which hDTR is expressed through eosinophil peroxidase locus (iPHIL) (Jacobsen et al., 2014). Administration of DT to *Sv*-infected iPHIL mice significantly reduced the numbers of eosinophils in duodenum and ileum LP (Figures 6A and 6B). Depletion of eosinophils did not affect egg load and *Sv* clearance, but abolished *Sv*-induced neuroprotection upon *spiB* infection (Figures 6C and 6D). This effect correlated with decreased levels of serum IL-4 and IL-13, lower frequency of Arg1+ MMs and reduced GI motility (Figures 6E–6G). In contrast, *Yp*-induced neuronal protection was not affected by depletion of eosinophils (Figures S4A and S4B).

Eosinophils are known to be major producers of IL-4 and IL-13, both of which can skew macrophages towards a tissue-protective phenotype (Liang et al., 2011; Wu et al., 2011). To evaluate the role of these cytokines produced by eosinophils in neuroprotection, we utilized $Epx^{\Delta Il4;Il13}$ mice, in which *Il4* and *Il13* genes are excised by eosinophil peroxidase promoter-driven *Cre* recombinase (Doyle et al., 2013). While *Sv*-induced eosinophilia was preserved in $Epx^{\Delta Il4;Il13}$ mice, subsequent *spiB* infection resulted in significant neuronal loss compared to wild-type control mice (Figures 6G and 6H). Consistently, absence of IL-4 and IL-13 in eosinophils resulted in their decreased serum levels as well as lower Arg1 expression by MMs and increased GI transit time (Figures 6J–6L). To assess whether increased numbers of eosinophils *per se* could also mediate neuronal protection, we utilized hydrodynamic overexpression of IL-5 (Nakagome et al., 2007). The treatment resulted in elevated frequencies of duodenum LP eosinophils (Figure S4C). However, when mice were challenged with *spiB*, we still observed a significant neuronal loss and no effect on the levels of Arg1+ MMs (Figure S4D and S4E). To investigate the exact localization of neuroprotective eosinophils, we performed a series of adoptive transfer experiments. Eosinophils derived from the ileum or duodenum of *Sv*-infected mice were transferred to congenic hosts that were subsequently challenged with *spiB* (Figure 6M). Transfer of $6{,}5\times10^5$ duodenum eosinophils resulted in neuronal protection (Figures 6N and 6O). In contrast, equal numbers of ileum eosinophils failed to induce a neuroprotective effect upon spiB challenge; these effects correlated with increased expression of IL-4 by eosinophils derived from duodenum *versus* ileum of *Sv*-infected mice and duodenum of host mice (Figures 6P, 6R and S4F). We then assessed whether direct administration of recombinant IL-4 or IL-13 could mediate neuronal protection following *spiB* infection. Repeated administration of recombinant IL-4 (rIL-4) or rIL-13 complex resulted in slightly delayed *spiB* clearance but prevented neuronal loss (Figures S4G and S4H). This result correlated

with increased frequencies of Arg1+ MMs (Figure S4I). These results suggest that secretion of IL-4 and/or IL-13 by activated duodenum eosinophils mediates distal neuroprotective effects by inducing Arg1 expression in MMs.

Similarly to eosinophils, tuft cells are known to respond to parasitic infections and initiate innate and adaptive type-2 responses in the intestine (Ting and von Moltke, 2019). Hence, we assessed whether their expansion and activation would result in neuro-protective effects by treating mice with succinate, which has been recently shown to induce tuft cell expansion and induction of type-2 responses in the small intestine (Nadjsombati et al., 2018; Schneider et al., 2018). Supplementation of succinate in the drinking water indeed led to increased frequencies of tuft cells in the epithelial compartment of the small intestine (Figure S4J), without impacting *spiB* clearance after subsequent oral infection. Nevertheless, this treatment did not prevent *spiB*-induced neuronal loss, increased transit time or result in higher levels of Arg1+ MMs (Figure S4K–S4N). Taken together, these data further suggest that only IL-4- and/or IL-13-producing eosinophils, enriched in the site of the infection, can mediate distal neuronal protection.

Long-term neuroprotection is maintained by modulation of hematopoietic progenitors

We wondered if macrophages differentiated from newly recruited monocytes can acquire a tissue-protective phenotype in response to activated eosinophils induced by *Sv* infection. We treated mice with anti-CSF1R antibody following *Sv* infection and waited for new monocytes to be recruited to the tissue and differentiate into MMs (Gabanyi *et al.*, 2016). Despite MM depletion post-*Sv* infection, subsequent *spiB* infection did not result in neuronal loss or reduced Arg1 expression by MMs when compared to isotype-treated animals, suggesting that long-term neuronal protection can be achieved by newly developed MMs (Figures S5A–S5C).

While eosinophils have been shown to survive up to 3 weeks within tissues, *Sv*-infection resulted in neuroprotection up to 24 weeks. Therefore, we investigated whether long-term neuronal protection is dependent on constant replenishment of eosinophils from bone marrow precursors. Based on recent reports (Kaufmann et al., 2018; Mitroulis et al., 2018), we hypothesized that initial *Sv* infection modulates bone marrow hematopoietic stem and progenitor cells, skewing them towards eosinophilic lineage. We analyzed bone marrow of *Sv*-infected mice and found that hematopoietic progenitors (LSK) cells, granulocyte macrophage progenitor (GMP) and eosinophil progenitor (EoP) cells were enriched up to 8 weeks post-infection (Figures 7A–7E). To assess whether changes in the bone marrow contribute to the increased frequencies of tissue eosinophils, and neuronal protection, we performed a series of bone marrow transfer experiments. First, we transferred 1000 long-term HSCs (LT-HSCs) from *Sv*-infected or non-infected donors to lethally irradiated congenic CD45.1+ hosts (Figures 7F and S5A). Host mice that received LT-HSCs from *Sv*-infected donors showed elevated levels of CD45.2+ eosinophils in the duodenum, but not ileum (Figures 7G and 7H). To assess whether skewing of bone marrow progenitors towards eosinophilic lineage can contribute to neuronal protection, we transferred 1×10^6 Lin^- cells from *Sv*-infected and non-infected donors to sublethally irradiated host mice, and after 12 weeks challenged them with *spiB* (Figure 7I). Regardless of the source of the bone marrow

progenitors, we observed significant neuronal loss and unaltered frequencies of Arg1+ MMs (Figures 7K and 7J).

Based on the above results, we hypothesized that in order to mediate their protective effect, newly recruited eosinophils need to be activated in the tissue microenvironment post-infection. To test this possibility, we transferred 1×10^6 Lin^- cells from *Sv*-infected donors to previously *Sv*-infected or non-infected lethally irradiated hosts, and after 12 weeks challenged them with *spiB* (Figure 7L). At day 5 post-infection we observed higher *spiB* burden in mice that were previously infected with *Sv*, but by day 7 both groups had cleared *spiB* (Figure S5E). We observed significant neuronal protection in bone marrow hosts that had been previously infected with *Sv*, which correlated with increased numbers of Arg1-expressing MMs (Figures 7M and 7N). To exclude the contribution of host MMs in this process we confirmed that ~90% of MMs were derived from the donor bone marrow (Figure 7O). These results indicate that *Sv* induces long-term restructuring of bone marrow precursors sustaining increased eosinophilic output that, together with post-infectious changes in the tissue microenvironment, induce a protective phenotype in tissue macrophages.

Discussion

Tissues can vary in their susceptibility to damage, regenerative capacity of their cells and in the impact caused by damage to host fitness; consequently, distinct disease tolerance mechanisms have been reported in different tissues and organs (Ayres, 2020; Martins *et al.*, 2019; Medzhitov *et al.*, 2012). The intestine is exposed to high amounts of microbes and potentially harmful substances, and consequently hosts highly regenerative cells like enterocytes, but also cells with low regenerative capacity such as neurons. While an increased regenerative capacity has been reported for enteric neurons, when compared to central nervous system (CNS) neurons (Furness, 2012), infection-induced neuronal loss can have a long-term impact in gut motility and host physiology (Balemans *et al.*, 2017; Matheis *et al.*, 2020; White *et al.*, 2018).

Our findings raise the possibility that infections early in life determine the number of enteric neurons in adult life. Pet store mice had significantly longer small intestines, which has been shown to depend on elevated levels of systemic IL-4 and -13 and in models of chronic helminth infections (Schneider *et al.*, 2018; Wong et al., 2007). Based on intestinal surface area and average neuronal densities, estimated total number of enteric neurons in the ileum is comparable between SPF and pet store mice, suggesting that free-living animals might maintain the state of tissue tolerance due to constant exposure to different pathogens. Further studies are needed to define the impact of infections on enteric neurons during development, as well as the neurochemical code of neurons lost, and restored during episodes of microbe exposure throughout the life of animals (Furness, 2012).

The mechanistic studies described here indicate that the intestinal tissue co-opted pathways induced by distinct pathogens into a convergent tissue macrophage phenotype that mediates enteric neuronal protection, aiding host fitness via intestinal motility and energy balance. Transcriptomic analysis of MMs suggests an evolutionary conserved gene signature similar

to human alternatively activated macrophages (Mages *et al.*, 2007; Pello *et al.*, 2012). Further studies into the epigenetic state of MMs might explain the mechanism behind the acquisition of a specific tissue-protective program independent of the type of infection. Our observations point to arginase-1 as a common downstream effector molecule instrumental for long-term neuronal protection. Expression of arginase-1 was required even in response to primary infection to *Sv* described here, similarly to what we had previously demonstrated in primary responses to *spiB* (Matheis *et al.*, 2020). Of note, at the timepoint analyzed here, we did not observe upregulation of Arg1 by MMs in response to *spiB*, a result somewhat discordant with our earlier study, which we attribute to the distinct timepoints analyzed and the focus on protein expression (here) versus RNA expression (Gabanyi *et al.*, 2016).

Our observations demonstrate how certain enteric infections induce durable beneficial effects utilizing pathways distinct from classical immunological memory. Another example of such process has been recently shown to rely on infection-induced changes in the gut microbiota composition resulting in enhanced resistance to other pathogens (Stacy et al., 2021). However, initial infections with enteric pathogens in our study never affected subsequent bacterial burden and pathogen clearance. Thus, these observations fit the main defining characteristics of disease tolerance (Ayres, 2020; Martins *et al.*, 2019; Medzhitov *et al.*, 2012).

Early studies on eosinophils have mostly focused on their role in clearance of helminths and on their contribution to allergic disorders. Their role in tissue tolerance shown in our study, as well as in a preprint study describing their contribution to the gut physiology (Shah et al., 2021) highlight previously unappreciated eosinophil functions. Mast cells and ILC2s are required for *Sv* clearance and have been shown to induce eosinophil accumulation (Mukai et al., 2017; Nussbaum et al., 2013). In our model this process was dependent on $CD4^+$ T cells, while depletion of mast cells did not impact neuronal protection. These observations suggest a division of labor between different innate cell subsets during type-2 responses: ILC2s and mast cells involved in pathogen resistance and eosinophils required for disease tolerance. The relatively short lifespan of eosinophils does not preclude their involvement in maintaining the state of tolerance in the long term. This effect was most likely due to epigenetic modulation of myelopoiesis progenitors skewing them towards eosinophilic lineage, a speculation that needs experimental demonstration. Of note, analogous long-term mechanisms of bone marrow restructuring have until now been described regarding macrophage's role in pathogen resistance (Kaufmann *et al.*, 2018; Mitroulis *et al.*, 2018). We hypothesize that certain infections can 'educate' HSCs in bone marrow resulting in increased eosinophilic output. As suggested by our comparison between duodenum *versus* ileal eosinophils, increased eosinophil bone marrow output must be accompanied by changes in the local microenvironment primed by initial infection, which then results in eosinophil activation and secretion of cytokines that modulate tissue macrophages. However, it remains open the question of whether a post-infectious microenvironment per se is sufficient to induce neuronal protection in the absence of bone marrow re-modelling. While the impact of disease tolerance mechanisms for host fitness have been demonstrated against a wide range of pathogens, our observations indicate that disease tolerance induced upon infection can have a long-term effect that benefit the host upon subsequent encounter with unrelated pathogens.

Limitations of the Study

While we have defined two main neuroprotective post-infectious mechanisms accounting for the preservation of the numbers and functionality of the ENS, our study did not address whether other classes of bacteria (e.g. Gram-positive) or pathogens (e.g. enteric viruses) induce similar mechanisms, and how long they would last.

STAR Methods

Lead Contact

Further information and requests for resources and reagents should be directed to and will be fulfilled by the Lead Contact, Daniel Mucida (mucida@rockefeller.edu).

Materials availability

Animal strains used in this study are available from The Jackson Laboratory or were provided by the indicated investigators. *cpa3*$^{\text{DTR-tdTomato}}$ were generated in this study and are available upon request.

Data and code availability

- RNA-seq data have been deposited at GEO and are publicly available as of the date of publication. Accession number is listed in the key resources table.
- This paper does not report original code.
- Any additional information required to reanalyze the data reported in this paper is available from the lead contact upon request.

Experimental Model and Subject Details

Mice—C57BL/6J (000664), Balb/c (000651), CD45.1 B6 (B6.SJL-Ptprc^{a} Pepc^{b}/BoyJ), LysM^{Cre} (B6.129P2-Lyz2$^{tm1(cre)Ifo}$/J, Arg$^{flox/flox}$ (C57BL/6-Arg1^{tm1Pmu}/J) and Il4;Il13$^{flox/flox}$ (B6.129P2(Cg)-Il4/Il13$^{tm1.Lky}$/J) were purchased from The Jackson Laboratories and maintained in our facilities. Adrb2$^{flox/flox}$ (Adrb2^{tm1Kry}) were generously provided by G. Karsenty, eoCRE (Epx$^{tm1.1(cre)Jlee}$) and iPHIL (Epx$^{tm2.1(HBEGF)Jlee}$) by E. Jacobsen, Hobit-Blimp-1 DKO (Hobit$^{-/-}$Blimp$^{flox/flox}$LCKCre$^{tg/+}$) by K. van Gisbergen. cpa3$^{\text{DTR-tdTomato}}$ mice were generated as described below. Pet store mice were purchased at a local pet store (Petco).

Mouse lines were interbred in our facilities to obtain the final strains described in the text. Genotyping was performed according to the protocols established for the respective strains by The Jackson Laboratories or personal communication with the donating investigators. Mice were maintained at the Rockefeller University animal facilities under specific pathogen-free conditions. Mice were fed a standard chow diet and used at 7–11 weeks of age for most experiments. Male and female (sex-matched) mice were used for all experiments. Animal care and experimentation were consistent with NIH guidelines and were approved by the Institutional Animal Care and Use Committee at the Rockefeller University.

Method Details

Infections

***Salmonella enterica* Typhimurium.:** For infections with Salmonella *spiB*, mice were pre-treated with a single dose of streptomycin (20 mg/mouse dissolved in 100 μl of DPBS) administered by oral gavage 18–24 h prior to infection. Mice were then orally inoculated with 10^9 CFU of *spiB*. A single aliquot of *spiB* was grown in 3 ml of LB overnight at 37 °C with agitation. Bacteria were then subcultured (1:300) into 3 ml of LB for 3.5 h at 37 °C with agitation and diluted to final concentration in 1 ml of DPBS.

Yersinia pseudotuberculosis.: *Y. pseudotuberculosis* (strain IP32777) was grown as previously described (Fonseca *et al.*, 2015). Briefly, a single aliquot of Yp was grown in 3 mL of 2xYT media overnight at 28 °C with vigorous agitation and diluted (1:10) to final concentration in DPBS. Mice were fasted for 12–16 h prior to infection with 10^8 CFU by oral gavage.

Strongyloides venezuelensis.: *S. venezuelensis* was maintained in our facility in NSG mice by subcutaneous infection with 1000 stage 3 (L3) larvae, resulting in chronic infection of this strain. For each experiment, feces of infected NSG mice were collected and spread on Whatman paper, which was places into a beaker with water and incubated at 28 °C for 2–3 days. Mice were infected subcutaneously with 700 L3 larvae in 200 μl water per mouse. *S. venezuelensis* was passaged periodically by infecting naïve adult NSG mice.

Heligmosomoides polygyrus.: Mice were infected by oral gavage with 200 third-stage larvae of H. polygyurs in 100 μl water.

Generation of *cpa3*$^{\text{DTR-tdTomato}}$ mice—*Cpa3*$^{\text{DTR-tdTomato}}$ knock-in mice were generated using CRISPR/Cas9 technology directly in C57BL/6 mice. Briefly, two guide RNA (gRNA) targeting exon 11 in the 3' UTR of the cpa3 locus were designed using the online CRISPR Design Tool. These gRNAs were cloned into a plasmid (Addgene) containing Cas9n. The plasmid was then co-injected into the pronucleus with a repair template plasmid (i.e. targeting vector, Addgene) containing an IRES-DTR-tdTomato fusion cassette. WT and knock-in genotypes were confirmed by PCR. DTR and IRES expression were confirmed using the repair template plasmid as a positive control. Insertion of the cassette into the correct locus was verified by using primers located inside the cassette and outside of the 3' and 5' homology regions, respectively.

Mouse treatments—Ivermectin (Milipore Sigma) was dissolved in DMSO at 100 mg/ml. 14 days after *Sv* infection, ivermectin was orally gavaged at 50 μg/mouse. 14 days after *Hp* infection ivermectin was injected subcutaneously at 20 mg/kg.

Diphtheria toxin (Sigma Aldrich) was reconstituted in DPBS. iPHIL mice were treated i.p. on indicated days at 15 ng/gram body weight. Cpa3-DTR mice were treated i.p. on indicated days at 300 μg/mouse.

For succinate treatment, mice were provided with 150mM sodium succinate hexahydrate (Alfa Aesar) *ad libitum* in drinking water for 14 days. As a control NaCl solution was given at 300 mM to match sodium molarity with succinate treatment.

For hydrodynamic gene delivery, pCAGGS vector containing mouse IL-5 coding sequence was used. Mice received hydrodynamic tail-vein injections of 100 ug plasmid DNA dissolved in lactated Ringer's solution (B. Braun) in a volume equal to 10% body weight (0.1 ml/g) within ± 5 s. As a control, empty pCAGGS expression vector was injected. Plasmid DNA was purified using EndoFree Plasmid Mega Kit (QIAGEN).

IL-4 or IL-13 complexes were prepared by incubating 5ug of recombinant IL-4 or IL-13 (PeproTech) with 25ug of anti-mouse IL-4 (clone 11B11, Bio X Cell) or IL-13 (clone eBio13A, ThermoFisher Scientific) for 5 mins at 4°C and injected i.p. at indicated timepoints in 100 ul PBS.

Antibodies against CD4 (Clone GK1.5, cat. # BE0003-1), CSF1R (Clone ASF98, cat. # BE0213) and IL-5 (Clone TRFK5, cat. # BE0198) and corresponding isotype controls were purchased from BioXCell. CD4 mAb was injected i.p. on indicated days at 200 μg/mouse/timepoint. IL-5 mAb was injected i.p. on indicated days at 500 μg/mouse/timepoint. CSF1R mAb was injected i.p. on indicated days at 50 mg/kg. Mice were previously habituated to i.p. injections for at least 5 days prior to the antibody treatments.

Bone marrow transfer—Bone marrow cells were harvested from WT $CD45.1^+$ or $CD45.2^+$ donors. Lineage-negative cells were isolated using direct lineage cell depletion kit (Miltenyi) according to manufacturer's protocol and r.o. injected into lethally irradiated (2 × 6 Gy) hosts at 1×10^6 cells/mouse along with 2×10^5 carrier bone marrow cells isolated from non-infected mice. LT-HSCs were sorted and r.o. injected into sublethally irradiated (6 Gy) hosts at 1000 cells/mouse. Mice were kept under sulfatrim diet for 2 weeks after the reconstitution and analyzed at indicated timepoints.

Metabolic cages—Body weight, food consumption and ambulatory activity was measured using the Phenomaster automated home cage phenotyping system (TSE systems, Bad Homburg, Germany). Mice were housed separately in a controlled environmental chamber set at 22 °C with 40 % humidity and with a 12 : 12 h light-dark cycle (lights on at 0700 and lights off at 1900). All mice were given food and water *ad libitum*. Mice were acclimatized in the metabolic cages for 24 h and thereafter metabolic values were automatically recorded for 72 h. Sampling interval for each mouse was 15 min with a settle time of 3 min. Raw values were analyzed using CalR (Mina et al., 2018). Data points represent the mean group value per hour. Error bars represent the group SEM per hour. For food consumption, p indicates the ANCOVA value with body weight as a covariable. For body weight and ambulatory activity, p indicates the two-way ANOVA value. n = 7 animals / group.

Flow cytometry and whole-mount immunofluorescence antibodies.—Antibodies against CD64-APC (Clone X54-5/7.1, cat. # 13906), CD4-BV605 (Clone RM4-5, cat. # 100548), CD150 (Clone TC15-12F12.2, cat. # 115921), CD48-APC (Clone HM480-1, cat. # 103411), Lineage Cocktail-PB (cat. # 133305) were purchases from BioLegend.

Antibodies against CD11b-APC-eFluor780 (Clone M1/70, cat. # 47-0112-82), FceR1-APC (Clone MAR1, cat. # 17-5898-80), CD45-PE-Cy7 (Clone 30-F11, cat. # 25-0451-82), CD45-AF700 (Clone 30-F11, cat. # 56-0451-82), CD45.1-PE-Cy7 (Clone A20, cat. # 25-0453-82), GATA-3-PE (Clone TWAJ, cat. # 12-9966-42), FOXP3-eFluor450 (Clone FJK-16s, cat. # 48-5773-82), MHC II-AF700 (Clone M5/114.15.2, cat. # 56-5321-82), Ly-6G-eFluor450 (Clone RB6-8C5, cat. # 48-5931-82), CD11c-AF488 (Clone N418, cat. # 53-0114-82), IL-4-APC (Clone 11B11, cat. # 17-7041-82), Arg1-PE-Cy7 (Clone A1exF5, cat. # 25-36-97-82), Ly6A/E(Sca-1)-PE (Clone D7, cat. # 12-5981-82), CD16/CD32-FITC (clone 93, cat. # 11-0161-82) were purchases from Thermo Fisher Scientific. Antibodies against CD11b-FITC (Clone M1/70, cat. # 553310), Siglec-F-APC-Cy7 (Clone E50-2440, cat. # 565527), -PE (Clone E50-2440, cat. # 552126) and -BV421 (Clone E50-2440, cat. # 56268), c-kit-PE-Cy7 (Clone 2B8, cat. # 558163), CD45.2-PerCP-Cy5.5 (Clone 104, cat. # 552950), CD45.2-AF700 (Clone 104, cat. # 560693), CD45R-FITC (Clone RA3-6B2, cat. # 553088), CD8a-AF488 (Clone 53-6.7, cat. # 557668), I-A/I-E-FITC (Clone M5/114.15.2, cat. # 553623), CD125-AF488 (Clone T21, cat. # 558533) were purchased from BD. Cell surface and intracellular antibodies were used at 1:200 and 1:100 dilution, respectively. Antibody against ANNA-1 was a gift from Dr. Vanda A. Lennon. Fluorophore-conjugated secondary antibody H&L goat anti-human-AF568 (Thermo Fisher Scientific) was used to detect anti-ANNA-1 antibody.

Intestine dissection—Mice were sacrificed and duodenum (1 cm moving distal from the gastroduodenal junction) or ileum (1 cm moving proximal from the ileocecal junction) was removed. For dissection of the *muscularis*, following the above procedures, the intestinal tissue was placed on a chilled aluminum block with the serosa facing up (Gabanyi *et al.*, 2016). Curved forceps were then used to carefully remove the *muscularis*. Tissue was then used for whole-mount imaging or flow cytometry.

Muscularis* processing for flow cytometry—Muscularis* was finely cut and digested in HBSS $Mg^{2+}Ca^{2+}$ + 5% FBS + 1x NaPyr + 25mM HEPES + 50 μg/ml DNaseI (Roche) + 400 U/ml Collagenase D (Roche) + 2.5 U/ml Dispase (Corning) at 37 °C. The *muscularis* was digested for 40 min. The tissue was then homogenized with an 18-gauge needle and filtered through a 70 μm cell strainer and washed with HBSS $Mg^{2+}Ca^{2+}$. The cells were incubated with Fc block and antibodies against the indicated cell surface markers in FACS buffer (PBS, 1% BSA, 10 mM EDTA, 0.02% sodium azide).

Bone marrow, spleen and lung processing—Bone marrow cells from femurs and spleen cells were passed through 70 μm filter and treated with red blood cell lysis buffer, followed by staining with fluorescently labeled antibodies. Lungs were dissected following perfusion with PBS, incubated for 45mins at 37°C in Collagenase A (Sigma Aldrich) and DNase I solution and passed through 70 μm filters.

Isolation of intraepithelial and lamina propria cells—Intraepithelial and lamina propria cells (eosinophils, T cells, mast cells, ILC2s and tuft cells) were isolated as previously described (Bilate et al., 2016). Briefly, sections of small intestines were harvested and washed in PBS and 1mM dithiothreitol (DTT) followed by 30 mM EDTA.

Intraepithelial cells were recovered from the supernatant of DTT and EDTA washes and mononuclear cells were isolated by gradient centrifugation using Percoll. Cells from lamina propria were obtained after collagenase 8 digestion of the tissue. Single-cell suspensions were then stained with fluorescently labeled antibodies for 30 min on ice.

Intracelluar staining for flow cytometry—Intranuclear staining for transcription factors was conducted using Foxp3 / Transcription Factor Staining Buffer Set according to manufacturer's instructions (eBioscience, USA). For analysis of IL-5 secretion, total mononuclear cells isolated from lamina propria were plated on 48-well plates and incubated at 37°C with 100 ng/mL phorbol 12-myristate 13-acetate (PMA, Sigma Aldrich) and 200 ng/mL ionomycin (Sigma) for 4 h. Golgi stop solution containing Monensin (2 mM, BD Biosciences) was added 1 h after PMA and ionomycin. Intracellular staining for cytokines was conducted in Perm/Wash buffer after fixation and permeabilization in Fix/Perm buffer (BD Biosciences, USA) according to kit instructions. Flow cytometry data were acquired on an LSR-II flow cytometer (Becton Dickinson, USA) and analyzed using FlowJo software package (Tri-Star, USA).

Gating strategies—For flow cytometric analysis following gating strategy was used to identify macrophages: single, live, myeloid cells (based on FSC, SSC and live/dead fixable dye Aqua stain), CD45+, CD11b+ and CD64+. Eosinophils: single, live, myeloid cells, CD45+, CD11b+ and Siglec-F+. Mast cells: single, live, myeloid cells, CD45+, CD117+ and FceR1+. LT-HSCs: single, live, Lin−, Sca1+, cKit+, CD150+, CD48−. ILC2s: single, live, CD45+, Lin−, CD127+, KLRG1+. Tuft cells: single, live, CD45−, EpCam+, Siglec-F+. For all cell types, B220+ and CD8a+ cells were excluded.

Eosinophil sorting—Following lamina propria cell isolation, cells were stained with fluorescently labelled antibodies against CD11b, CD11c, Gr1 and MHCII (Geslewitz et al., 2018). Cells (single, live, CD45+, CD11b+, Gr1+, CD11c−, MHCII−) were then sorted using a FACSAria™ cell sorter flow cytometer (Becton Dickinson) and subsequently transferred by retro-orbital injection at numbers indicated in Figure 5.

RNA-Seq Library Preparation—Sorted muscularis macrophages (1000 cells) were lysed in guanidine thiocyanate buffer (TCL buffer, Qiagen) supplemented with 1% β-mercaptoethanol. RNA was isolated by solid-phase reversible immobilization bead cleanup using RNAClean XP beads (Agentcourt), reverse-transcribed and amplified as described (Trombetta et al., 2014). Uniquely barcoded libraries were prepared using Nextera XT kit (Illumina) following manufacturer's instructions. Sequencing was performed on an Illumina NextSeq500 for a total yield of 400M reads.

RNA-Seq Analysis—Raw fastq files were processed by using the mouse transcriptome (gencode M23) with the kallisto (v0.46) software. Analysis of transcript quantification was performed at the gene level by using the sleuth (v0.30) package for R. To spot statistically significantly expressed genes between group pairs, we used the wald-test function. Genes with false discovery rate less than 0.01 and 2 or 4 log2 fold-change were used in downstream analysis. The batch effect was removed from the expression matrix by using the removebatcheffect function available in the limma package. Gene set enrichment analysis

(GSEA) was performed by using signature gene sets in gmt format and a pre-ranked gene list by log2 fold-change between two groups as input for the fgsea.

Cytokine quantification—After centrifugation of peripheral blood, the serum samples were immediately aliquoted and stored at 4 °C until the experiment was conducted. The concentrations of IL-4 and IL-13 were measured once after collection of each individual samples by using the cytometric bead array assay (BD Biosciences) according to the manufacturer's instructions.

CFU counting—Fecal pellets from *spiB- or Yp*-infected mice were weighed and then disrupted in 400 mL of DPBS. Serial dilutions were made from the original suspension and then 5 ml of each dilution was plated onto Salmonella-Shigella or 2xYT-Irgasan plates, respectively. The plates were then incubated overnight, and the number of black colonies were counted for the serial dilution with the clearest delineation of single units. This number was then multiplied by the dilution factor and by 80 to give the number of colony-forming units (CFU) in the original suspension. CFU numbers were then divided by the original fecal pellet weight to give the number of CFU per mg of feces.

Quantification of *Sv* eggs in feces—Fecal pellets from *Sv*-infected mice were weighed and then disrupted in 400 µl of DPBS. 100 µl of iodine solution was added to increase the visibility of fecal eggs. Eggs in small portions of each sample were counted under a microscope, and the number of eggs per gram of feces was determined for each sample.

Intestine motility measurements—For measurement of total intestinal transit time, mice were given an oral gavage of 6% carmine red (Sigma-Aldrich) dissolved in 0.5 % methylcellulose (prepared in sterile 0.9% NaCl). Total intestinal transit time was measured as the time from oral gavage it took for mice to pass a fecal pellet that contained carmine.

Neuronal imaging and counting quantification—After dissection muscularis was pinned down on a plate coated with Sylgard and then fixed overnight with 4 % PFA. After washing in DPBS whole mount samples were then permeabilized first in 0.5 % Triton X-100 (perm buffer) for 2 h at room temperature (RT) with gentle shaking. Samples were then blocked for 2 h in blocking buffer (5 % bovine serum albumin and 5 % goat serum in perm buffer) for 2 h at RT with gentle agitation. Anti-ANNA-1 antibody was added to the blocking buffer at appropriate concentrations and incubated for 2 days at 4°C. After primary incubation the tissue was washed 4 times in perm buffer and then incubated in blocking buffer with secondary antibody for 2–3 h at RT. Samples were again washed 4 times in perm buffer and then mounted with FluoroMount G on slides with coverslips. Slides were kept in the dark at 4 °C until they were imaged. A minimum of 5–10 images were randomly acquired across a piece of whole-mount *muscularis*. These images were then opened in Fiji, and the cell counter was used to count the number of ANNA-1+ cells in a given field. This number was then multiplied by a factor of 2.95 (20x objective) or 3.125 (25x objective), to calculate the number of counted neurons per square millimeter (mm^2). The average of 8–10 images was then calculated and plotted. Whole-mount intestine samples were imaged on an inverted LSM 880 NLO laser scanning confocal and multiphoton microscope (Zeiss) and on an inverted TCS SP8 laser scanning confocal microscope (Leica).

CG-SMG dissections and cFos staining—Mice were cervically dislocated and a midline incision was made; the viscera were removed out of the peritoneal cavity. The superior mesenteric artery was located by identifying the intersection of the descending aorta and left renal artery. Fine forceps and microdissection scissors were used to remove the CG-SMG which is wrapped around the superior mesenteric artery and associated lymphatic vessels. CG-SMG samples were washed in cold 1x PBS and fixed overnight at 4 °C in 4% PFA. CG-SMG samples were then washed four times in 1x PBS at room temperature and blocked overnight in 5% Normal Donkey Serum with 0.5% Triton X-100/0.05% Tween-20/4 μg heparin (PTxwH) at 4 °C. Samples then incubated with anti-cFos (1:500; Cell Signaling Technologies, 2250S) and anti-TH (1:200; Milipore; AB1542) for 48 hours at 4 °C. Samples were washed four times in PTxwH at room temperature and incubated with highly cross-adsorbed donkey anti-rabbit AF647 (Invitrogen A31573) and donkey anti-sheep AF568 (Invitrogen; A21099) antibodies at 4 °C for 48 hours (rotating). Samples were washed four times in PTxwH at room temperature and mounted in Fluoromount G. TH staining was used to identify the sympathetic neurons and number of cFos+ nuclei were counted in multiple z-stack images with confocal microscope. ImageJ Cell Counter plugin was used to count the cFos+ nuclei and data were not normalized to area or volume. Each data point represents the total number of cFos+ cells per CG-SMG.

Intestine neuronal quantification: neurons per ganglion.—A myenteric ganglion was defined as a continuous group of ANNA1+ cells that are separated by less than 15 μm in distance. Only complete ganglia were counted per field of view. Thus, the following ganglia were excluded: 1. Ganglia that were truncated; 2. No clear separation (>15 μm) was noted between the last ANNA1+ cell and the edge of the field of view. In the case of single ANNA1+ cells that are separated by 15μm on all sides, this was counted as extraganglionic. The number of quantifiable ganglia was averaged across a minimum of 10 images per gut segment per animal.

Quantification and Statistical Analysis

Statistical analysis—Significance levels indicated are as follows: * $p < 0.05$, ** $p < 0.01$, *** $p < 0.001$, **** $p < 0.0001$. All data are presented as mean ± SD or mean ± SEM. At least two independent experiments were performed throughout in this study. All statistical tests used were two-tailed. Multivariate data were analyzed by one-way ANOVA and Tukey's multiple comparisons post hoc test. Comparisons between two conditions were analyzed by unpaired Student's t test. GraphPad PRISM version 9 was used for generation of graphs and statistics.

Supplementary Material

Refer to Web version on PubMed Central for supplementary material.

Acknowledgements

We thank all Mucida Lab members and Rockefeller University employees for their continuous assistance; A. Rogoz and S. Gonzalez for the maintenance of mice, RU Bio-imaging Research Center for assistance with image acquisition analysis and Tiago B.R. Castro for assembling the RNAseq analysis platform for the lab. We thank E. Jacobsen for providing iPHIL and $Epx^{tm1.1(cre)Jlee}$ mouse strains, M. Merad for the anti-CSF1R hybridoma, V.

Lenon for anti-Anna-1 antibody, S. Galli and K. Matsushita for the *Sv* larvae, I. Brodsky for *Yp*, J. Lafaille for *H. polygyrus* larvae, Jun-ichi Miyazaki for pCAGGS-IL5 plasmid, J. von Moltke for suggestions in the succinate experiments and P. Cohen for CLAMS cage experiments. We also thank Victora and Lafaille labs for fruitful discussions. This work was supported by NIH Transformative R01DK116646 and R01DK126407, Kenneth Rainin Foundation, Food Allergy FARE/FASI Consortium, NIH R01DK126407 (D.M.). T.A. is a Human Frontier of Science Program postdoctoral fellow. B.A. is a Simons Foundation junior fellow. D.M. is an investigator of the Howard Hughes Medical Institute.

References

Abolins S, King EC, Lazarou L, Weldon L, Hughes L, Drescher P, Raynes JG, Hafalla JCR, Viney ME, and Riley EM (2017). The comparative immunology of wild and laboratory mice, Mus musculus domesticus. Nature communications 8, 14811. 10.1038/ncomms14811.

Ariotti S, Hogenbirk MA, Dijkgraaf FE, Visser LL, Hoekstra ME, Song JY, Jacobs H, Haanen JB, and Schumacher TN (2014). T cell memory. Skin-resident memory CD8(+) T cells trigger a state of tissue-wide pathogen alert. Science 346, 101–105. 10.1126/science.1254803. [PubMed: 25278612]

Ayres JS (2020). The Biology of Physiological Health. Cell 181, 250–269. 10.1016/j.cell.2020.03.036. [PubMed: 32302569]

Balemans D, Mondelaers SU, Cibert-Goton V, Stakenborg N, Aguilera-Lizarraga J, Dooley J, Liston A, Bulmer DC, Vanden Berghe P, Boeckxstaens GE, and Wouters MM (2017). Evidence for long-term sensitization of the bowel in patients with post-infectious-IBS. Scientific reports 7, 13606. 10.1038/s41598-017-12618-7. [PubMed: 29051514]

Bilate AM, Bousbaine D, Mesin L, Agudelo M, Leube J, Kratzert A, Dougan SK, Victora GD, and Ploegh HL (2016). Tissue-specific emergence of regulatory and intraepithelial T cells from a clonal T cell precursor. Sci Immunol 1, eaaf7471. 10.1126/sciimmunol.aaf7471. [PubMed: 28783695]

De Schepper S, Verheijden S, Aguilera-Lizarraga J, Viola MF, Boesmans W, Stakenborg N, Voytyuk I, Schmidt I, Boeckx B, Dierckx de Casterle I, et al. (2018). Self-Maintaining Gut Macrophages Are Essential for Intestinal Homeostasis. Cell 175, 400–415 e413. 10.1016/j.cell.2018.07.048. [PubMed: 30173915]

Desai P, Janova H, White JP, Reynoso GV, Hickman HD, Baldridge MT, Urban JF Jr., Stappenbeck TS, Thackray LB, and Diamond MS (2021). Enteric helminth coinfection enhances host susceptibility to neurotropic flaviviruses via a tuft cell-IL-4 receptor signaling axis. Cell. 10.1016/j.cell.2021.01.051.

Doyle AD, Jacobsen EA, Ochkur SI, Willetts L, Shim K, Neely J, Kloeber J, Lesuer WE, Pero RS, Lacy P, et al. (2013). Homologous recombination into the eosinophil peroxidase locus generates a strain of mice expressing Cre recombinase exclusively in eosinophils. Journal of leukocyte biology 94, 17–24. 10.1189/jlb.0213089. [PubMed: 23630390]

Esterhazy D, Canesso MCC, Mesin L, Muller PA, de Castro TBR, Lockhart A, ElJalby M, Faria AMC, and Mucida D (2019). Compartmentalized gut lymph node drainage dictates adaptive immune responses. Nature 569, 126–130. 10.1038/s41586-019-1125-3. [PubMed: 30988509]

Fonseca DM, Hand TW, Han SJ, Gerner MY, Glatman Zaretsky A, Byrd AL, Harrison OJ, Ortiz AM, Quinones M, Trinchieri G, et al. (2015). Microbiota-Dependent Sequelae of Acute Infection Compromise Tissue-Specific Immunity. Cell 163, 354–366. 10.1016/j.cell.2015.08.030. [PubMed: 26451485]

Furness JB (2012). The enteric nervous system and neurogastroenterology. Nature reviews. Gastroenterology & hepatology 9, 286–294. 10.1038/nrgastro.2012.32. [PubMed: 22392290]

Furness JB, Rivera LR, Cho HJ, Bravo DM, and Callaghan B (2013). The gut as a sensory organ. Nature reviews. Gastroenterology & hepatology 10, 729–740. 10.1038/nrgastro.2013.180. [PubMed: 24061204]

Gabanyi I, Muller PA, Feighery L, Oliveira TY, Costa-Pinto FA, and Mucida D (2016). Neuro-immune Interactions Drive Tissue Programming in Intestinal Macrophages. Cell 164, 378–391. 10.1016/j.cell.2015.12.023. [PubMed: 26777404]

Geslewitz WE, Percopo CM, and Rosenberg HF (2018). FACS isolation of live mouse eosinophils at high purity via a protocol that does not target Siglec F. Journal of immunological methods 454, 27–31. 10.1016/j.jim.2017.12.001. [PubMed: 29253503]

Holschneider DP, Bradesi S, and Mayer EA (2011). The role of experimental models in developing new treatments for irritable bowel syndrome. Expert review of gastroenterology & hepatology 5, 43–57. 10.1586/egh.10.88. [PubMed: 21309671]

Iniesta V, Gomez-Nieto LC, Molano I, Mohedano A, Carcelen J, Miron C, Alonso C, and Corraliza I (2002). Arginase I induction in macrophages, triggered by Th2-type cytokines, supports the growth of intracellular Leishmania parasites. Parasite immunology 24, 113–118. 10.1046/j.1365-3024.2002.00444.x. [PubMed: 11982856]

Jacobsen EA, Lesuer WE, Willetts L, Zellner KR, Mazzolini K, Antonios N, Beck B, Protheroe C, Ochkur SI, Colbert D, et al. (2014). Eosinophil activities modulate the immune/inflammatory character of allergic respiratory responses in mice. Allergy 69, 315–327. 10.1111/all.12321. [PubMed: 24266710]

Kaufmann E, Sanz J, Dunn JL, Khan N, Mendonca LE, Pacis A, Tzelepis F, Pernet E, Dumaine A, Grenier JC, et al. (2018). BCG Educates Hematopoietic Stem Cells to Generate Protective Innate Immunity against Tuberculosis. Cell 172, 176–190 e119. 10.1016/j.cell.2017.12.031. [PubMed: 29328912]

Liang HE, Reinhardt RL, Bando JK, Sullivan BM, Ho IC, and Locksley RM (2011). Divergent expression patterns of IL-4 and IL-13 define unique functions in allergic immunity. Nature immunology 13, 58–66. 10.1038/ni.2182. [PubMed: 22138715]

Lilla JN, Chen CC, Mukai K, BenBarak MJ, Franco CB, Kalesnikoff J, Yu M, Tsai M, Piliponsky AM, and Galli SJ (2011). Reduced mast cell and basophil numbers and function in Cpa3-Cre; Mcl-1fl/fl mice. Blood 118, 6930–6938. 10.1182/blood-2011-03-343962. [PubMed: 22001390]

Mackay LK, Minnich M, Kragten NA, Liao Y, Nota B, Seillet C, Zaid A, Man K, Preston S, Freestone D, et al. (2016). Hobit and Blimp1 instruct a universal transcriptional program of tissue residency in lymphocytes. Science 352, 459–463. 10.1126/science.aad2035. [PubMed: 27102484]

Mages J, Dietrich H, and Lang R (2007). A genome-wide analysis of LPS tolerance in macrophages. Immunobiology 212, 723–737. 10.1016/j.imbio.2007.09.015. [PubMed: 18086374]

Maizels RM (2020). Regulation of immunity and allergy by helminth parasites. Allergy 75, 524–534. 10.1111/all.13944. [PubMed: 31187881]

Marple A, Wu W, Shah S, Zhao Y, Du P, Gause WC, and Yap GS (2017). Cutting Edge: Helminth Coinfection Blocks Effector Differentiation of CD8 T Cells through Alternate Host Th2- and IL-10-Mediated Responses. Journal of immunology 198, 634–639. 10.4049/jimmunol.1601741.

Martins R, Carlos AR, Braza F, Thompson JA, Bastos-Amador P, Ramos S, and Soares MP (2019). Disease Tolerance as an Inherent Component of Immunity. Annual review of immunology 37, 405–437. 10.1146/annurev-immunol-042718-041739.

Matheis F, Muller PA, Graves CL, Gabanyi I, Kerner ZJ, Costa-Borges D, Ahrends T, Rosenstiel P, and Mucida D (2020). Adrenergic Signaling in Muscularis Macrophages Limits Infection-Induced Neuronal Loss. Cell 180, 64–78 e16. 10.1016/j.cell.2019.12.002. [PubMed: 31923400]

Medzhitov R, Schneider DS, and Soares MP (2012). Disease tolerance as a defense strategy. Science 335, 936–941. 10.1126/science.1214935. [PubMed: 22363001]

Mina AI, LeClair RA, LeClair KB, Cohen DE, Lantier L, and Banks AS (2018). CalR: A Web-Based Analysis Tool for Indirect Calorimetry Experiments. Cell metabolism 28, 656–666 e651. 10.1016/j.cmet.2018.06.019. [PubMed: 30017358]

Mitroulis I, Ruppova K, Wang B, Chen LS, Grzybek M, Grinenko T, Eugster A, Troullinaki M, Palladini A, Kourtzelis I, et al. (2018). Modulation of Myelopoiesis Progenitors Is an Integral Component of Trained Immunity. Cell 172, 147–161 e112. 10.1016/j.cell.2017.11.034. [PubMed: 29328910]

Mukai K, Karasuyama H, Kabashima K, Kubo M, and Galli SJ (2017). Differences in the Importance of Mast Cells, Basophils, IgE, and IgG versus That of CD4(+) T Cells and ILC2 Cells in Primary and Secondary Immunity to Strongyloides venezuelensis. Infection and immunity 85. 10.1128/IAI.00053-17.

Muller PA, Koscso B, Rajani GM, Stevanovic K, Berres ML, Hashimoto D, Mortha A, Leboeuf M, Li XM, Mucida D, et al. (2014). Crosstalk between muscularis macrophages and enteric neurons regulates gastrointestinal motility. Cell 158, 300–313. 10.1016/j.cell.2014.04.050. [PubMed: 25036630]

Nadjsombati MS, McGinty JW, Lyons-Cohen MR, Jaffe JB, DiPeso L, Schneider C, Miller CN, Pollack JL, Nagana Gowda GA, Fontana MF, et al. (2018). Detection of Succinate by Intestinal Tuft Cells Triggers a Type 2 Innate Immune Circuit. Immunity 49, 33–41 e37. 10.1016/j.immuni.2018.06.016. [PubMed: 30021144]

Nakagome K, Dohi M, Okunishi K, Tanaka R, Kouro T, Kano MR, Miyazono K, Miyazaki J, Takatsu K, and Yamamoto K (2007). IL-5-induced hypereosinophilia suppresses the antigen-induced immune response via a TGF-beta-dependent mechanism. Journal of immunology 179, 284–294. 10.4049/jimmunol.179.1.284.

Nussbaum JC, Van Dyken SJ, von Moltke J, Cheng LE, Mohapatra A, Molofsky AB, Thornton EE, Krummel MF, Chawla A, Liang HE, and Locksley RM (2013). Type 2 innate lymphoid cells control eosinophil homeostasis. Nature 502, 245–248. 10.1038/nature12526. [PubMed: 24037376]

O'Leary CE, Schneider C, and Locksley RM (2019). Tuft Cells-Systemically Dispersed Sensory Epithelia Integrating Immune and Neural Circuitry. Annual review of immunology 37, 47–72. 10.1146/annurev-immunol-042718-041505.

Ohman L, and Simren M (2010). Pathogenesis of IBS: role of inflammation, immunity and neuroimmune interactions. Nature reviews. Gastroenterology & hepatology 7, 163–173. 10.1038/nrgastro.2010.4. [PubMed: 20101257]

Pello OM, De Pizzol M, Mirolo M, Soucek L, Zammataro L, Amabile A, Doni A, Nebuloni M, Swigart LB, Evan GI, et al. (2012). Role of c-MYC in alternative activation of human macrophages and tumor-associated macrophage biology. Blood 119, 411–421. 10.1182/blood-2011-02-339911. [PubMed: 22067385]

Schneider C, O'Leary CE, von Moltke J, Liang HE, Ang QY, Turnbaugh PJ, Radhakrishnan S, Pellizzon M, Ma A, and Locksley RM (2018). A Metabolite-Triggered Tuft Cell-ILC2 Circuit Drives Small Intestinal Remodeling. Cell 174, 271–284 e214. 10.1016/j.cell.2018.05.014. [PubMed: 29887373]

Shah K, Ignacio A, Bernier-Latmani J, Köller Y, Coakley G, Moyat M, Hamelin R, Armand F, Wong NC, Ramay H, et al. (2021). Small Intestinal Resident Eosinophils Maintain Gut Homeostasis Following Microbial Colonisation. bioRxiv, 2021.2001.2030.428930. 10.1101/2021.01.30.428930.

Silveira MR, Nunes KP, Cara DC, Souza DG, Correa A Jr., Teixeira MM, and Negrao-Correa D (2002). Infection with Strongyloides venezuelensis induces transient airway eosinophilic inflammation, an increase in immunoglobulin E, and hyperresponsiveness in rats. Infection and immunity 70, 6263–6272. [PubMed: 12379705]

Soares MP, Gozzelino R, and Weis S (2014). Tissue damage control in disease tolerance. Trends in immunology 35, 483–494. 10.1016/j.it.2014.08.001. [PubMed: 25182198]

Stacy A, Andrade-Oliveira V, McCulloch JA, Hild B, Oh JH, Perez-Chaparro PJ, Sim CK, Lim AI, Link VM, Enamorado M, et al. (2021). Infection trains the host for microbiota-enhanced resistance to pathogens. Cell 184, 615–627 e617. 10.1016/j.cell.2020.12.011. [PubMed: 33453153]

Ting HA, and von Moltke J (2019). The Immune Function of Tuft Cells at Gut Mucosal Surfaces and Beyond. Journal of immunology 202, 1321–1329. 10.4049/jimmunol.1801069.

Trombetta JJ, Gennert D, Lu D, Satija R, Shalek AK, and Regev A (2014). Preparation of Single-Cell RNA-Seq Libraries for Next Generation Sequencing. Current protocols in molecular biology 107, 4 22 21–17. 10.1002/0471142727.mb0422s107. [PubMed: 24984854]

Tsolis RM, Townsend SM, Miao EA, Miller SI, Ficht TA, Adams LG, and Baumler AJ (1999). Identification of a putative Salmonella enterica serotype typhimurium host range factor with homology to IpaH and YopM by signature-tagged mutagenesis. Infection and immunity 67, 6385–6393. [PubMed: 10569754]

Vivier E, Artis D, Colonna M, Diefenbach A, Di Santo JP, Eberl G, Koyasu S, Locksley RM, McKenzie ANJ, Mebius RE, et al. (2018). Innate Lymphoid Cells: 10 Years On. Cell 174, 1054–1066. 10.1016/j.cell.2018.07.017. [PubMed: 30142344]

White JP, Xiong S, Malvin NP, Khoury-Hanold W, Heuckeroth RO, Stappenbeck TS, and Diamond MS (2018). Intestinal Dysmotility Syndromes following Systemic Infection by Flaviviruses. Cell. 10.1016/j.cell.2018.08.069.

Wong T, Hildebrandt MA, Thrasher SM, Appleton JA, Ahima RS, and Wu GD (2007). Divergent metabolic adaptations to intestinal parasitic nematode infection in mice susceptible or resistant to obesity. Gastroenterology 133, 1979–1988. 10.1053/j.gastro.2007.09.006. [PubMed: 18054569]

Wu D, Molofsky AB, Liang HE, Ricardo-Gonzalez RR, Jouihan HA, Bando JK, Chawla A, and Locksley RM (2011). Eosinophils sustain adipose alternatively activated macrophages associated with glucose homeostasis. Science 332, 243–247. 10.1126/science.1201475. [PubMed: 21436399]

Highlights:

- Bacteria-induced neuroprotection is mediated by β-2AR signaling in macrophages.
- Helminth-induced neuroprotection relies on eosinophil-derived IL-4 and -13.
- Pet store mice display similar neuroprotection as previously infected SPF mice.
- Post-infectious bone marrow and tissue environment maintain long-term neuroprotection.

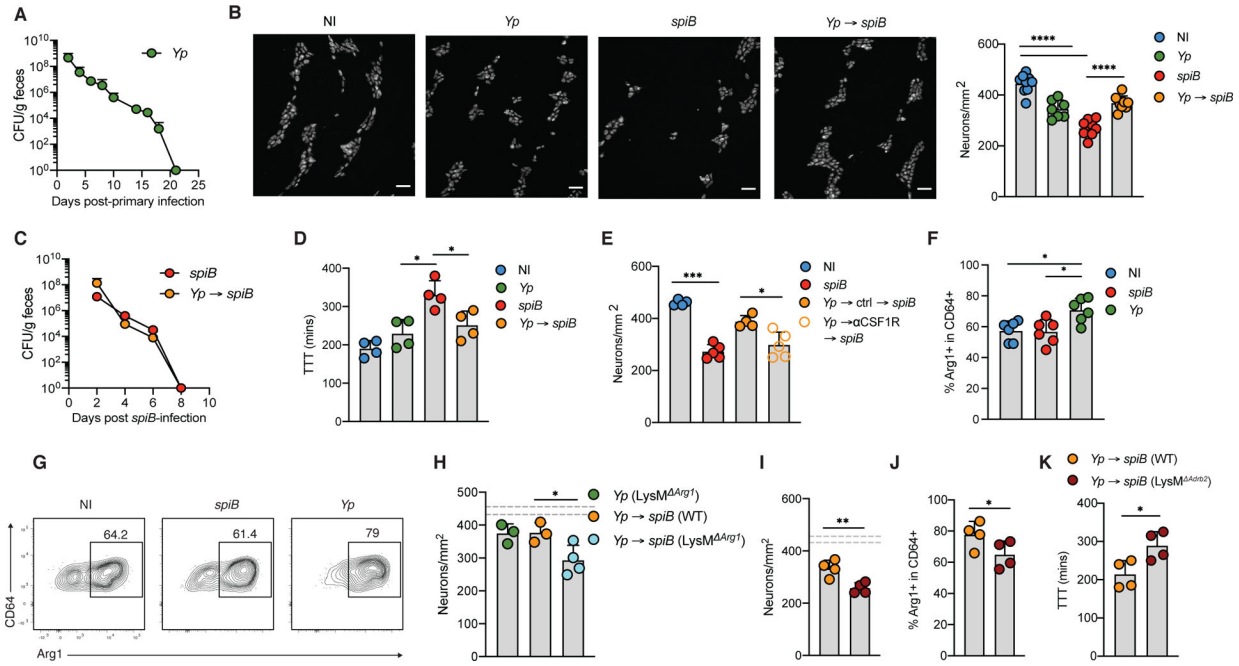

Figure 1. *Y. pseudotuberculosis* infection induces neuronal protection during subsequent infection.

(A-D) C57BL/6J mice were orally gavaged with PBS (non-infected, NI), 10^9 colony-forming units (CFU) of *Salmonella* Typhimurium *spiB*, 10^8 CFU of *Y. pseudotuberculosis* (*Yp*) only or 10^8 CFU of *Yp* and 21 days later with 10^9 CFU of *spiB*. (A) Quantification of fecal *Yp* CFU. (B) Neuronal quantification in the ileum myenteric plexus assessed by IF staining of ANNA-1 on day 10 post-*spiB* infection. Left, representative images; Scale bars, 50 μm. (C) Quantification of fecal *spiB* CFU. (D) Total GI transit time measured at 12 days post infection (dpi). (E) C57BL/6J mice were orally gavaged with PBS, *spiB* or *Yp*. At 20 dpi *Yp*-infected mice were treated with anti-CSF1R or IgG isotype control, followed by oral gavage with *spiB*. Ileum myenteric plexus neurons were quantified at 7 dpi. (F and G) Flow cytometry analysis of Arg1-expressing macrophages isolated from ileum muscularis at 14 dpi with *Yp* or *spiB*. (H) Quantification of ileum myenteric plexus neurons of LysM$^{\Delta Arg1}$ mice and WT littermates orally gavaged with *Yp* only or followed by *spiB* infection 21 days later. (I-K) LysM$^{\Delta Adrb2}$ (Cre+) mice and WT (Cre−) littermates were orally gavaged with *Yp* and 21 days later with *spiB*. (I) Neuronal quantification of ileum myenteric plexus 7 days post-*spiB* infection. (J) Arg1 expression by macrophages in ileum *muscularis* at 7 dpi as determined by flow cytometry. (K) Total gastrointestinal (GI) transit time at 12 dpi. Dashed lines indicate the range of day 7 enteric neuron numbers defined by mean ± SEM of a set of control non-infected C57BL/6J mice (n=25). Data is from 2 pooled independent experiments (3–5 mice per condition, A-C and F) or one out of two representative experiments (D-E and G-K). See also Figure S1.

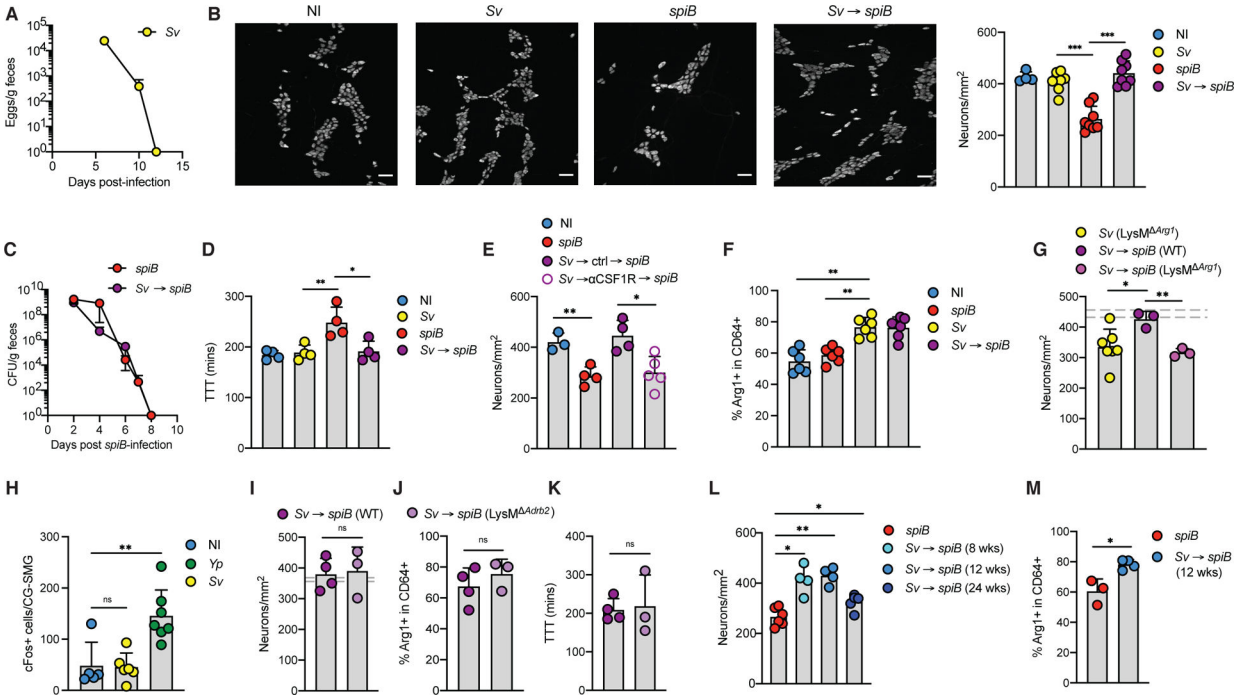

Figure 2. *S. venezuelensis* infection induces long-term neuronal protection during subsequent infection.

(A-D) C57BL/6J mice were s.c. injected with water and then orally gavaged with PBS (non-infected, NI) or infected with *spiB*, *Sv* only or *Sv* and 14 days later with *spiB*. (A) Quantification of fecal *Sv* eggs. (B) Right, Neuronal quantification in the ileum myenteric plexus assessed by IF staining using ANNA-1 on day 8 post- *spiB* infection or 14 days post-*Sv* infection. Left, representative images; Scale bars, 50 μm. (C) Quantification of fecal *spiB* CFU. (D) Total GI transit time measured at 10 dpi. (E) C57BL/6J mice were orally gavaged with PBS or infected with *spiB* or *Sv*. At 14 dpi *Sv*-infected mice were treated with anti-CSF1R or IgG isotype control, followed by oral gavage with *spiB*. Ileum myenteric plexus neurons were quantified 7 days post-*spiB* infection. (F) Flow cytometry analysis of Arg1-expressing macrophages isolated from ileum muscularis at 14 dpi with *Sv* or *spiB*. (G) Neuronal quantification of ileum myenteric plexus of LysM$^{\Delta Arg1}$ (Cre+) mice and WT (Cre−) littermates orally gavaged with *Sv* only or followed by *spiB* infection 14 days later. (H) Number of cFos+ neurons in CG-SMG 3 days after *Yp* infection, 7 days after *Sv* infection and in non-infected controls. (I-K) LysM$^{\Delta Adrb2}$ mice and WT littermates were orally gavaged with *Sv* and 14 days later with *spiB*. (I) Quantification of ileum myenteric plexus neurons 7 days post-*spiB* infection. (J) Arg1 expression by macrophages in ileum myenteric plexus at 7 dpi. (K) Total GI transit time at 10 dpi. (L and M) C57BL/6J mice were orally gavaged with *spiB* only or s.c. injected with *Sv* and 8, 12 or 24 weeks later infected with *spiB*. (L) Ileum myenteric plexus neurons were quantified 10 days post-*spiB* infection. (M) Arg1 expression by macrophages in ileum myenteric plexus at 7 dpi as determined by flow cytometry. (G and I) Dashed lines indicate the range of day 7 enteric neuron numbers defined by mean ± SEM of a set of control non-infected C57BL/6J mice (n=25). Data is from 2 pooled independent experiments (3–5 mice per condition, A-C and H) or one out of two representative experiments (D-G and I-M). See also Figure S2.

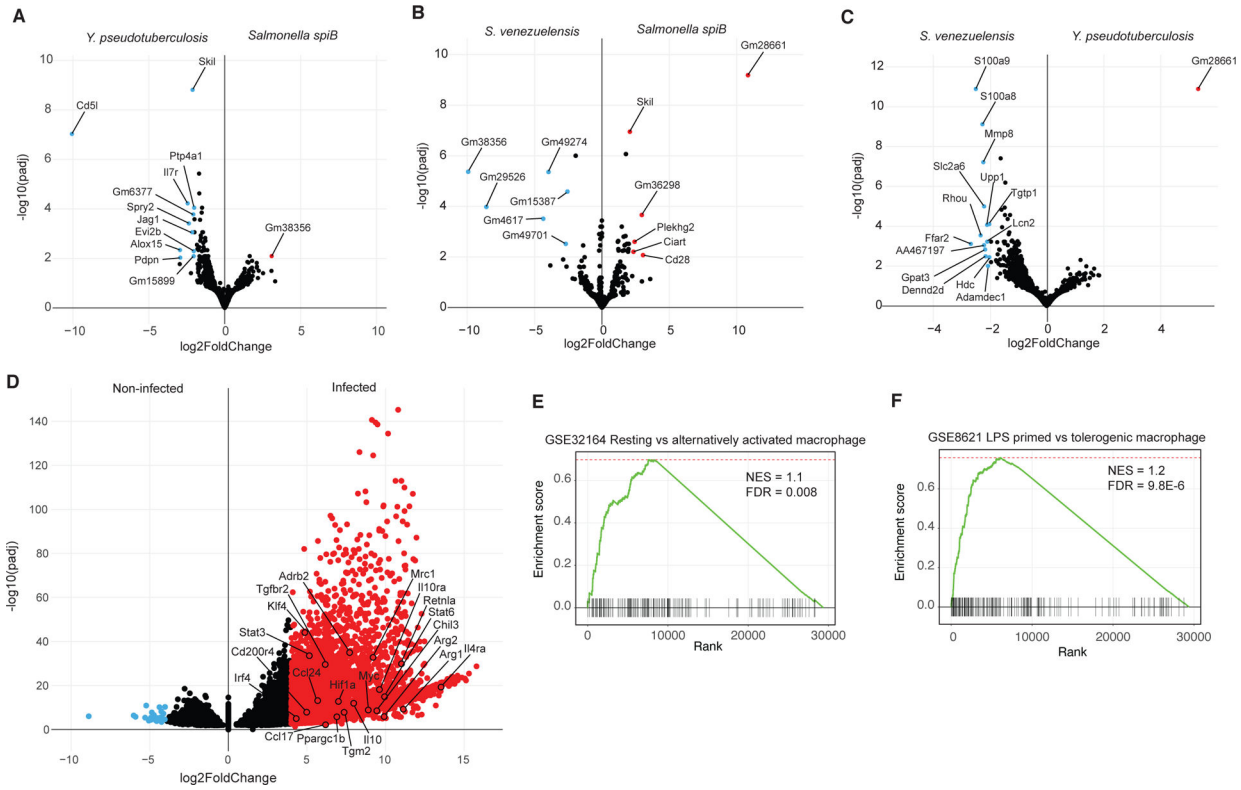

Figure 3. Transcriptomic analysis of MMs.

(A-F) C57BL/6J mice were s.c. injected with water (non-infected, NI) or infected with *spiB*, *Sv* or *Yp*. Ileum MMs were sorted for RNA-seq at 14dpi. (A-D) Volcano plots showing comparisons between (A) *Yp* and *spiB* group, (B) *Sv* and *spiB* group, (C) *Sv* and *Yp* group and (D) infected (all infections pooled) and non-infected group. All significantly regulated genes (FDR<0.01) are colored. (E-F) GSEA of MM gene signature from all infected mice in indicated publicly available datasets. See also Table S1.

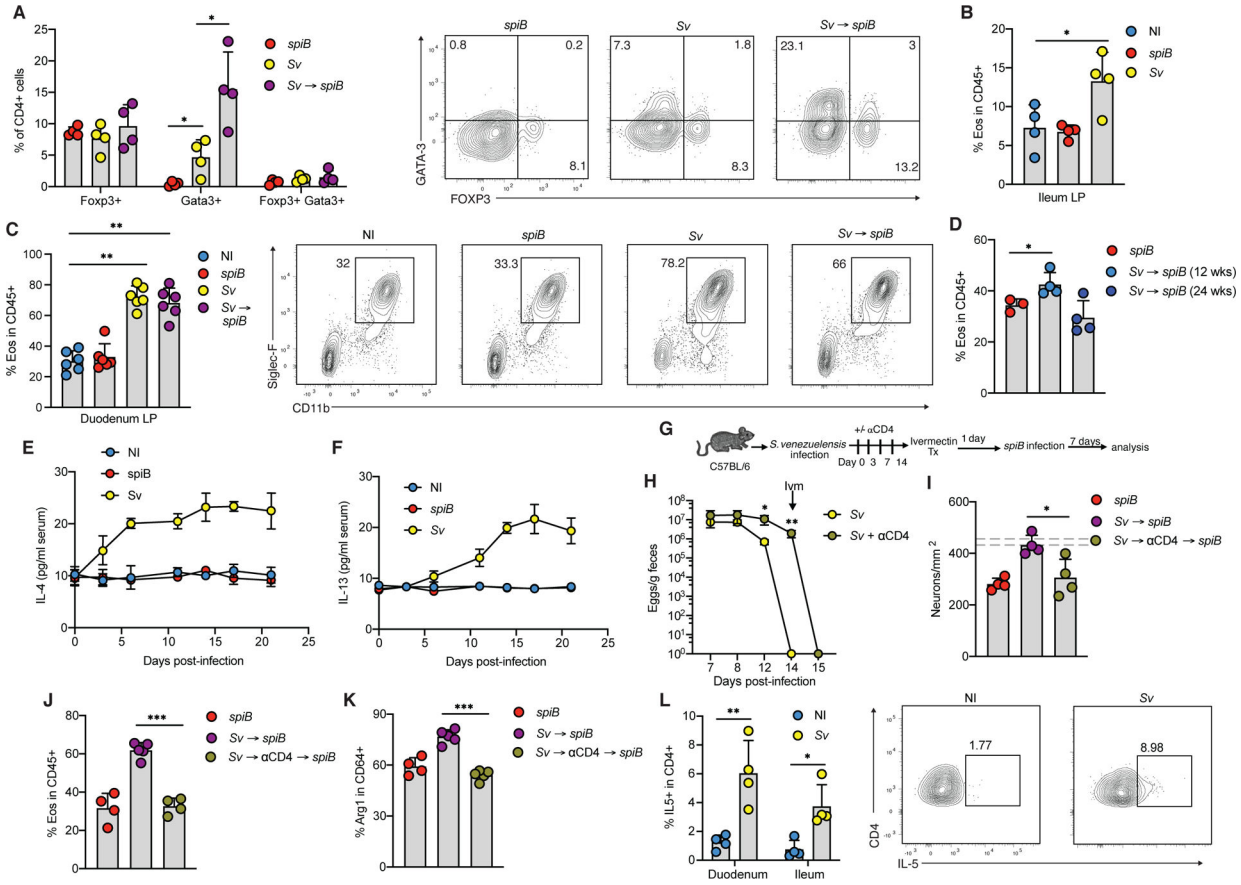

Figure 4. Immune response to *S. venezuelensis* is associated with neuronal protection during subsequent infection.

(A-F) C57BL/6J mice were s.c. injected with water (non-infected, NI) or infected with *spiB*, *Sv* only or *Sv* and 14 days later with *spiB*. (A) Flow cytometric intranuclear analysis of $CD4^+$ T cells in lamina propria (LP) expressing indicated transcription factors 2 days post-*spiB* infection. (B and C) Frequency of ileum (B) and duodenum (C) LP eosinophils at 14 dpi with *Sv*. (D) Frequency of duodenum LP eosinophils in mice infected with *spiB* only and *Sv* followed by *spiB* 12 or 24 weeks later and analyzed at 7 dpi. (E and F) Serum levels of IL-4 (E) and IL-13 (F) measured over time post-infection with *spiB* or *Sv*. (G) Experimental design for (H-K). (H-K) C57BL/6J mice were infected with *spiB* or *Sv*. On indicated days *Sv*-infected mice were treated with anti-CD4 antibody, followed by treatment with ivermectin and oral gavage with *spiB*. (H) Quantification of fecal *Sv* eggs. (I) Quantification of ileum myenteric plexus neurons 7 days post-*spiB* infection. Dashed lines indicate the range of day 7 enteric neuron numbers defined by mean ± SEM of a large set of control C57BL/6J mice. (J) Frequency of duodenum LP eosinophils at 7 dpi. (K) Arg1 expression by ileum myenteric plexus macrophages at 7 dpi. (L) C57BL/6J mice were subcutaneously injected *Sv* or PBS. IL-5 expression in $CD4^+$ T cells was determined after 4-hour *in vitro* stimulation of duodenum LP cells with PMA and ionomycin at 21 dpi. Data in (C) is from 2 pooled independent experiments (3 mice per condition). All other data is from one representative out of two independent experiments with 3–4 mice per condition. See also Figure S3.

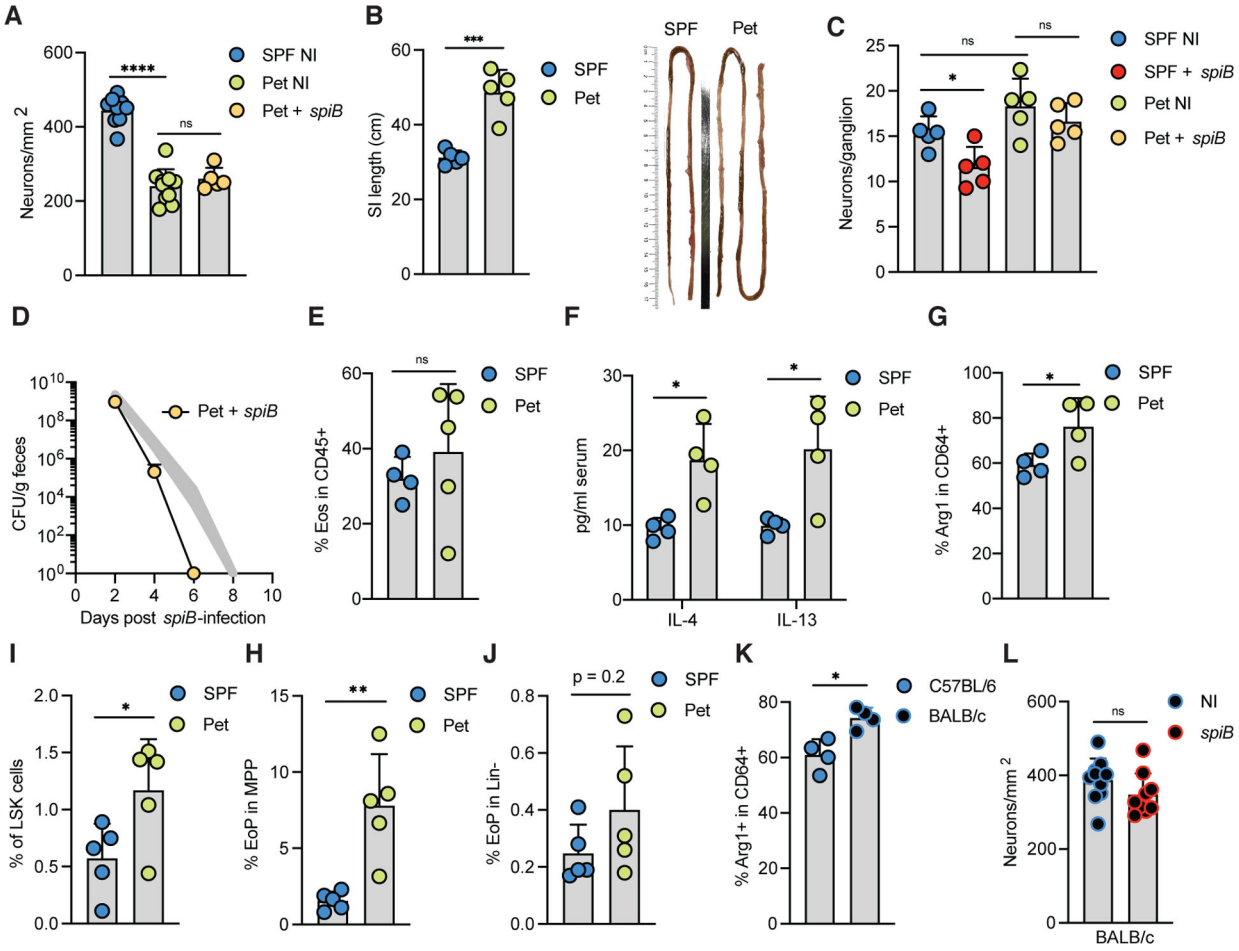

Figure 5. Pet store mice are resistant to neuronal loss upon *spiB* infection.

Pet store mice were analyzed at steady-state (A-C and E-J) or 7 days post *spiB*-infection (A, C and D). (A) Quantification of ileum myenteric plexus neurons. (B) Small intestine length. (C) Number of neuron per ganglion within the ileum myenteric plexus. (D) Quantification of fecal *spiB* CFU. Shaded area indicates range of *spiB* CFU numbers defined by mean ± SEM from a large set of control SPF mice. (E) Frequency of duodenum LP eosinophils. (F) Serum levels of IL-4 and IL-13. (G) Frequency of Arg1-expressing ileum myenteric plexus macrophages. (H-J) Frequencies of indicated bone marrow progenitor cell subsets. (K) Frequency of Arg1-expressing ileum MMs in non-infected BALB/c and C57BL/6 mice. (L) BALB/c mice were orally gavaged with PBS (non-infected, NI) or *spiB.* Ileum myenteric plexus neurons were quantified at 15 dpi. Data is from one representative out of 2 independent experiments (B-J) or 2 pooled independent experiments with 3–5 mice per condition (A and K).

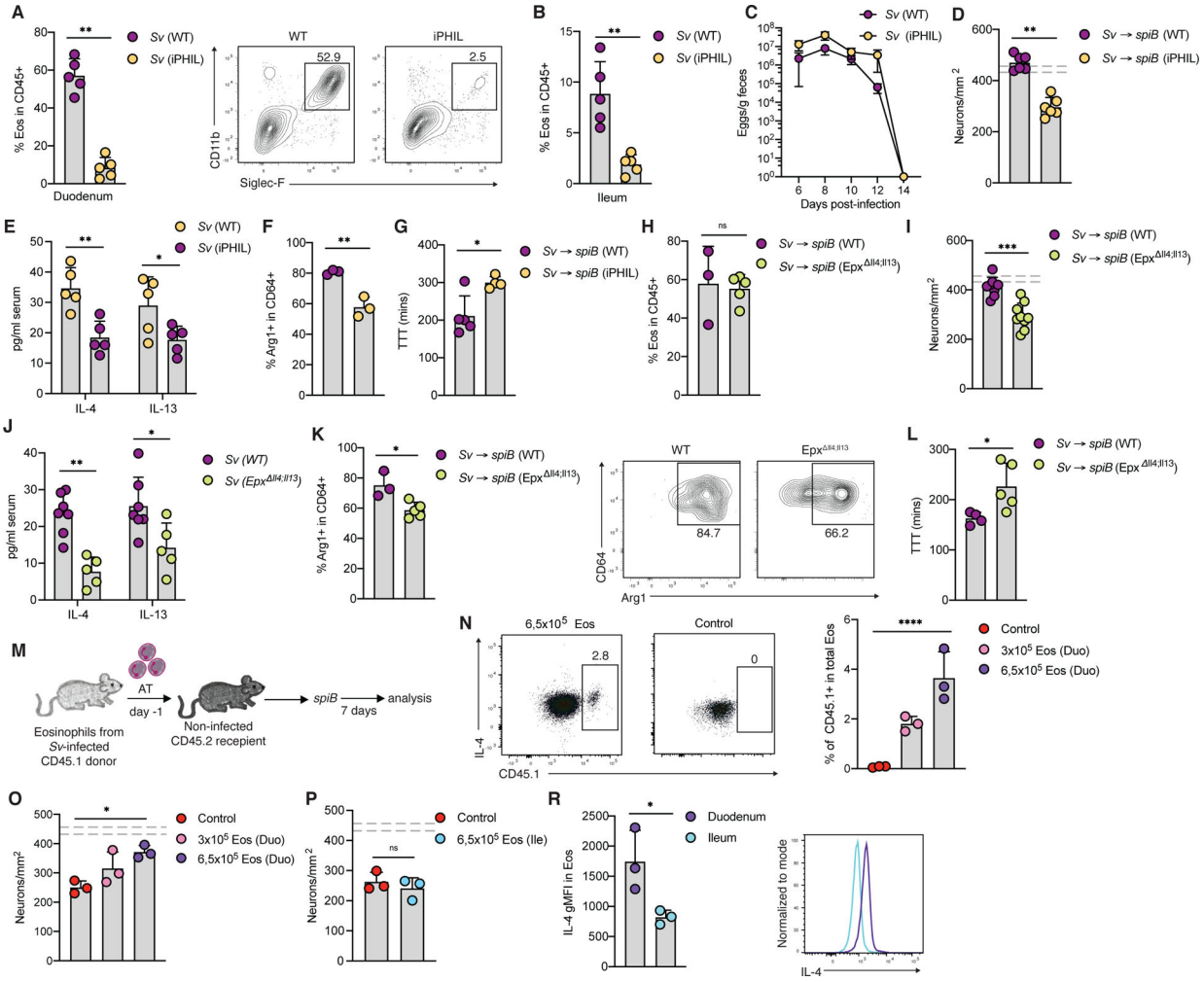

Figure 6. IL-4 and IL-13 producing eosinophils mediate *Sv*-induced neuronal protection.

(A-C) iPHIL mice and WT littermates were infected with *Sv* and treated with DT on day 0, 1, 4, 6 and 8 post-infection. Analysis was performed at 10 dpi. (A and B) Frequency of duodenum (A) and ileum (B) LP eosinophils. (C) Quantification of fecal *Sv* eggs. (D-F) iPHIL mice and WT littermates were infected with *Sv* and treated with DT on day 0, 1, 4, 7, 10, 13, 16 and 18 post-infection. On day 14 post-*Sv* infection mice were orally gavaged with *spiB*. (D) Quantification of ileum myenteric plexus neurons at 7 dpi. (E) Serum levels of IL-4 and IL-13 at 7 dpi. (F) Arg1 expression by ileum myenteric plexus macrophages at 7 dpi. (G) Total GI transit time measured 10 days post-*spiB* infection. (H-L) $Epx^{\Delta Il4;Il13}$ mice or WT littermates were infected with *Sv* larvae and 14 days later with *spiB*. (H) Frequency of duodenum LP eosinophils at 7 dpi. (I) Quantification of ileum myenteric plexus neurons at 7 dpi. (J) Serum levels of IL-4 and IL-13 7 dpi. (K) Arg1 expression by ileum myenteric plexus macrophages at 7 dpi. (L) Total GI transit time measured 10 days post-*spiB* infection. (M) Experimental design for (N-P). (N-P) C57BL/6J CD45.2 mice received indicated numbers of eosinophils isolated from duodenum or ileum LP of CD45.1 mice infected with *Sv* 7 days earlier. Recipient mice were subsequently infected with *spiB*. (N) Frequency of donor $CD45.1^+$ duodenum eosinophils found in LP of recipient mice at 7

dpi. Quantification of ileum myenteric plexus neurons in mice receiving duodenum (O) or ileum (P) eosinophils 7 days post-*spiB* infection. (R) C57BL/6J mice were infected with *Sv*. Expression of IL-4 was measured in duodenum and ileum eosinophils 7 days post-infection. Dashed lines indicate the range of day 7 enteric neuron numbers defined by mean ± SEM of a set of control non-infected C57BL/6J mice (n=25). Data is from one representative out of 2 independent experiments (A-H and J-R) or 2 pooled independent experiments with 3–5 mice per condition (I). See also Figure S4.

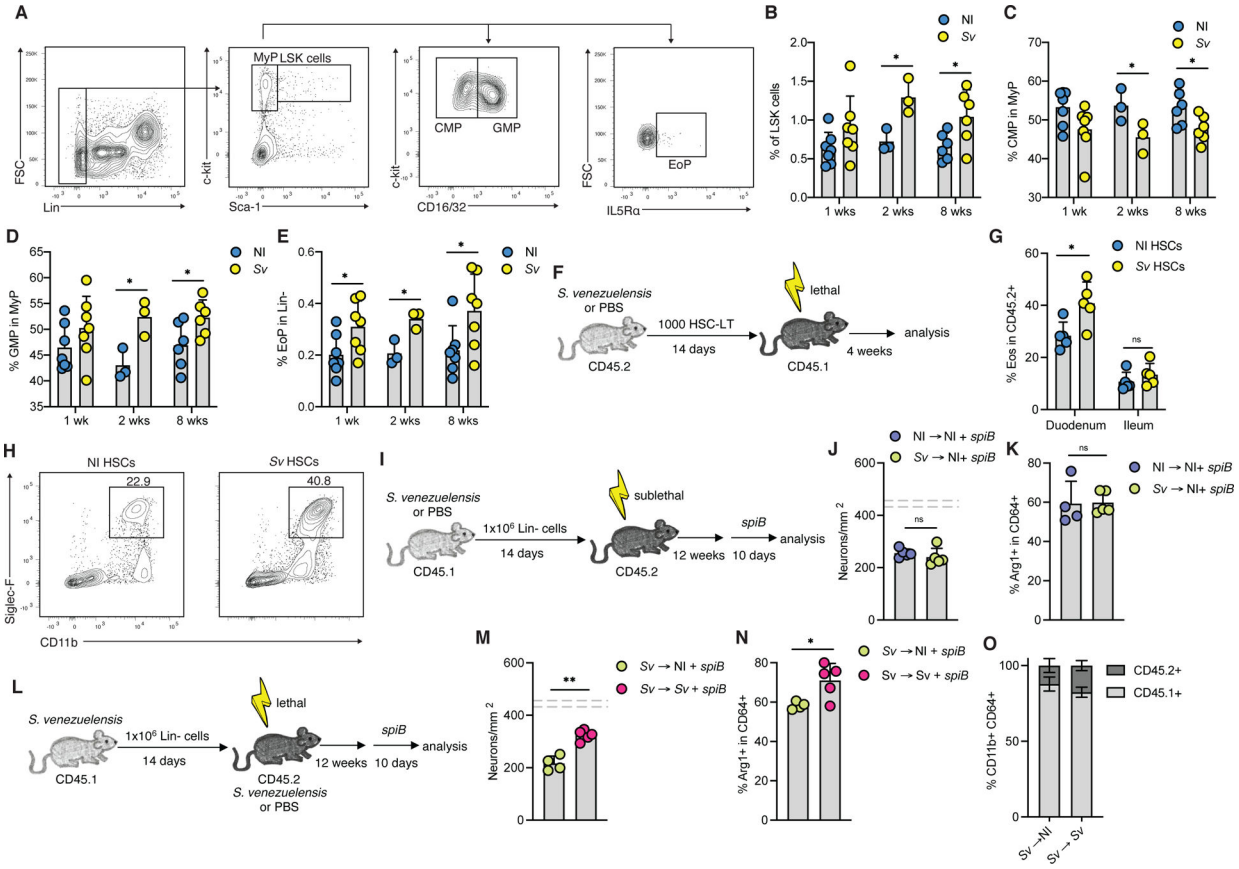

Figure 7. Long-term neuroprotection is maintained by modulation of hematopoietic progenitors.

(A-E) C57BL/6J mice were infected with *Sv.* Frequencies of indicated bone marrow progenitor cell subsets 1, 2 and 8 weeks post-*Sv* infection. (F) Experimental design for (G and H). (G and H) Lethally irradiated CD45.1$^+$ host mice received 1000 LT-HSCs isolated from donor CD45.2$^+$ mice s.c. injected with water or infected with *Sv* 14 days earlier. (G and H) Frequency of CD45.2$^+$ duodenum and ileum LP eosinophils 4 weeks post-HSC transfer. (I) Experimental design for (J and K). Sublethally irradiated CD45.2$^+$ host mice received 1×10^6 lineage-negative bone marrow cells isolated from donor CD45.1$^+$ mice s.c. injected with water or infected with *Sv* 14 days earlier. After 12 weeks, host mice were infected with *spiB*. (J) Quantification of ileum myenteric plexus neurons at 7 dpi. (K) Arg1 expression by ileum myenteric plexus macrophages at 10 dpi. (L) Experimental design for (M-O). (M-O) CD45.2$^+$ host mice were s.c. injected with water or *Sv* larvae and 14 days later lethally irradiated and i.v. injected with 1×10^6 lineage-negative bone marrow cells isolated from donor CD45.1$^+$ mice infected with *Sv* 14 days earlier. After 12 weeks, host mice were challenged with *spiB*. (M) Quantification of ileum myenteric plexus neurons at 10 dpi. (N) Arg1 expression by ileum myenteric plexus macrophages at 10 dpi. (O) Frequency of CD45.1$^+$ and CD45.2$^+$ ileum myenteric plexus macrophages in host mice. Data is from one representative out of 2 independent experiments (G-O) or 2 pooled independent experiments with 3–5 mice per condition (B-E). See also Figure S5.